GC-MS-based ^{13}C metabolic flux analysis resolves the parallel and cyclic glucose metabolism of *Pseudomonas putida* KT2440 and *Pseudomonas aeruginosa* PAO1

Michael Kohlstedt, Christoph Wittmann*

Institute of Systems Biotechnology, Saarland University, Campus A 1.5, 66123 Saarbrücken, Germany

ABSTRACT

The genus *Pseudomonas* comprises approximately 200 species with numerous isolates that are common inhabitants of soil, water, and vegetation and has been of particular interest for more than one hundred years. Here, we present a novel approach for accurate, precise and convenient ^{13}C metabolic flux analysis of these and other microbes possessing periplasmic glucose oxidation and a cyclic hexose metabolism, which forms the recently discovered EDEMP cycle. This complex cyclic architecture cannot be resolved by common metabolic flux workflows, which rely on GC-MS-based labelling analysis of proteinogenic amino acids. Computational analyses revealed that this limitation can be overcome by three parallel labelling experiments on specific tracers, i.e., [1–^{13}C], [6–^{13}C] and 50% [^{13}C$_6$] glucose, with additional consideration of labelling information from glucose and glucosamine. Glucose and glucosamine display building blocks from cellular glycogen, peptidoglycan and lipopolysaccharides, reflect the pools of glucose6-phosphate and fructose6-phosphate in the heart of the EDEMP cycle and as we show, can be precisely assessed in biomass hydrolysates by GC-MS. The developed setup created 534 mass isotopomers and enabled high-resolution flux analysis of the cell factory *Pseudomonas putida* KT2440 and the human pathogen *P. aeruginosa* PAO1. The latter strain oxidized approximately 90% of its glucose into gluconate via the periplasmic route, whereas only a small fraction of substrate was phosphorylated and consumed via the cytoplasmic route. The oxidative pentose phosphate pathway was completely inactive, indicating the essentiality of the Entner-Doudoroff pathway and recycling of triose units into anabolic precursors.

In addition to pseudomonads, many microbes operate a cyclic hexose metabolism, which becomes more accessible to flux analysis with this approach. In this regard, the presented approach displays a valuable extension of the available set of flux methods for these types of bacteria.

1. Introduction

^{13}C metabolic flux analysis (MFA) is a powerful technology used to quantify intracellular fluxes in microbial systems, i.e., *in vivo* enzymatic rates (Buescher et al., 2015). Over the years, this approach has provided unique insights into important microorganisms, such as *Escherichia coli* (Fischer and Sauer, 2003; He et al., 2017; Wada et al., 2017)*, Corynebacterium glutamicum* (Bartek et al., 2011; Hoffmann et al., 2018), *Basfia succiniciproducens* (Becker et al., 2013; Lange et al., 2017)*, Vibrio natriegens* (Long et al., 2017), and *Bacillus subtilis* (Kohlstedt et al., 2014; Schilling et al., 2007).

State-of-the-art ^{13}C MFA uses ^{13}C isotope cultures of the cells of interest, whose cellular metabolite ^{13}C-labelling patterns are analysed in terms of the isotopic substrates as input for a software-based flux calculation (Zamboni et al., 2009). An essential part of a successful

workflow is a precise and informative ^{13}C analysis. Different variants of mass spectrometry (MS) (Heinzle et al., 2008; Nöh et al., 2007; Wittmann and Heinzle, 2001a; Yang et al., 2006) and nuclear magnetic resonance (NMR) spectroscopy (Boisseau et al., 2013; Choudhary et al., 2011; Millard et al., 2017; Reardon and Isern, 2017) have been successfully used in ^{13}C MFA studies. Although each of these individual techniques and sometimes their combinations have proven value, gas chromatography-MS (GC-MS) is the most frequently used technology for ^{13}C flux measurements (Wittmann, 2007). A particularly attractive feature of GC-MS is its analytical power to accurately and quickly quantify the ^{13}C-labelling pattern of various amino acids from the cell protein (Christensen et al., 2000; Dauner and Sauer, 2000). Due to the easy accessibility of protein in almost all studied cells and the information richness of the accessible amino acids, this type of analysis has become routine in many laboratories, if not a "gold standard" for

---

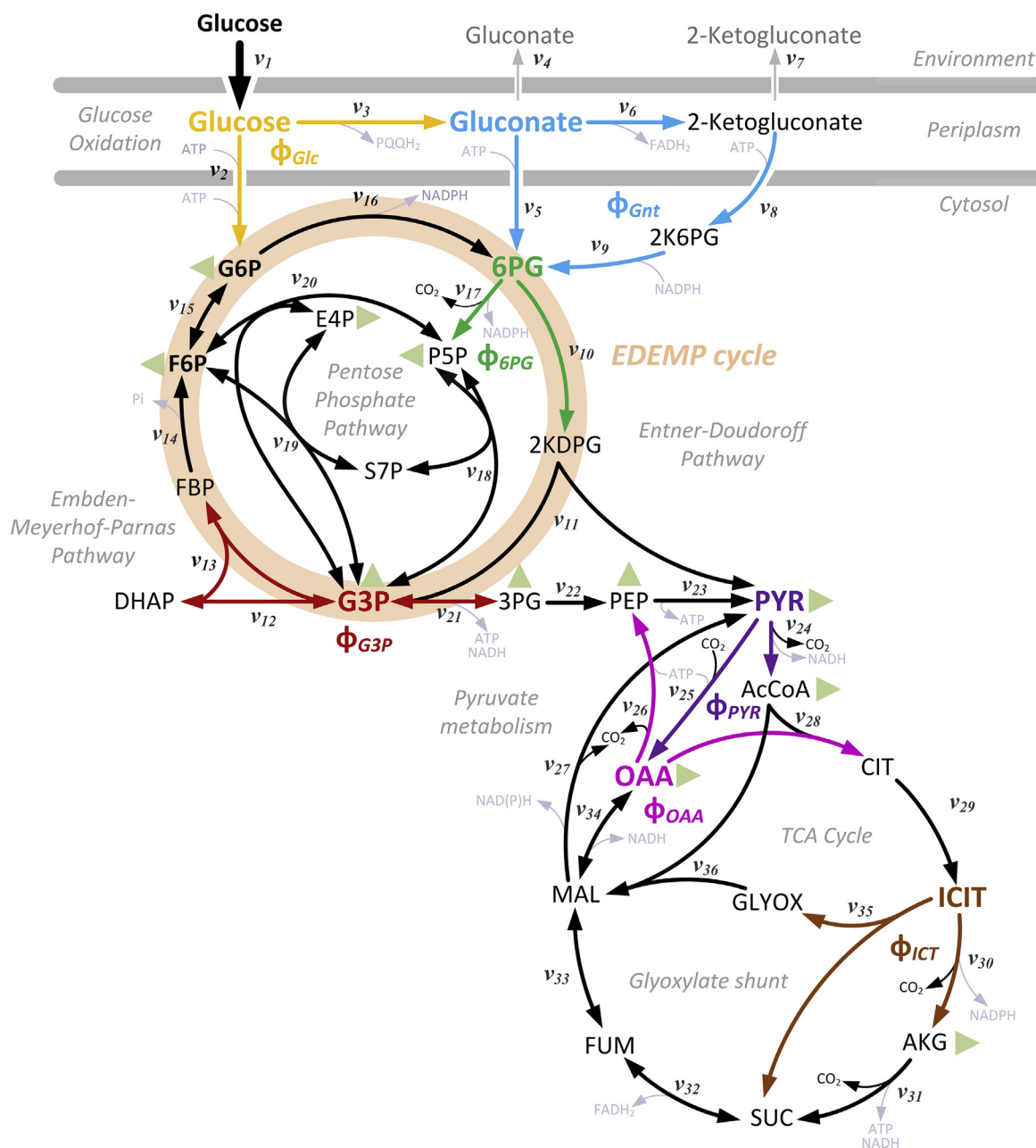**Fig. 1. Metabolic network of the central carbon metabolism of *Pseudomonas putida* KT2440.** This microbe lacks a functional phosphofructokinase and does not use the linear Embden-Meyerhof-Parnas (EMP) pathway for hexose degradation (Romano and Conway, 1996). Instead, it possesses the Entner-Doudoroff (ED) pathway, the pentose phosphate (PP) pathway, and a rich set of cytoplasmic and periplasmic oxidation and phosphorylation reactions, while the available subset of EMP pathway reactions allows operation in only the gluconeogenic direction. The reactions are merged into the EDEMP cycle, which assembles enzymes from the ED, the EMP and the PP pathways into a unique metabolic architecture (Nikel et al., 2015). As a consequence, the substrate glucose can be either phosphorylated in the cytoplasm or oxidized in the periplasm. The latter path forms gluconate and subsequently 2-ketogluconate, both of which can also be phosphorylated into 6-phosphogluconate (6PG) and 6-phospho-2-ketogluconate (2K6PG), respectively, leading to three entry pathways into the core metabolism.

[13]C-labelling analysis in flux studies of microorganisms (Adler et al., 2013; Barbier et al., 2014; Fischer and Sauer, 2003; Lee and Kim, 2005; Price et al., 2006). When needed, parallel experiments with different tracers can be conducted to enhance flux resolution (Becker et al., 2008; Crown and Antoniewicz, 2013; Hayakawa et al., 2018; Kind et al., 2013; Shirai et al., 2005; Wittmann and Heinzle, 2002; Wittmann et al., 2007).

However, *Pseudomonas* bacteria and related microbes have not been analysed in full detail using common GC-MS workflows and even different tracers (Blank et al., 2008; del Castillo et al., 2007; Fuhrer et al., 2005; Klingner et al., 2015). To date, GC-MS-based flux studies of pseudomonads have provided only partial insights and cannot resolve

important properties of cellular redox and energy metabolism (Berger et al., 2014; Lassek et al., 2016; Opperman and Shachar-Hill, 2016). This limitation is due to the fact that these bacteria possess a glycolytic metabolism that is different from (and more complex than) that of most other microbes (Entner and Doudoroff, 1952; Romano and Conway, 1996). Pseudomonads operate a cyclic metabolism, the so-called EDEMP cycle (Fig. 1), which merges activities belonging to the Embden-Meyerhof-Parnas (EMP) pathway, the Entner-Doudoroff (ED) pathway, and the pentose phosphate (PP) pathway into a complex architecture, as recently demonstrated for *Pseudomonas putida* KT2440 (Nikel et al., 2015). Interestingly, such a metabolism is also found in other microbes (Gosselin et al., 2001; Portais et al., 1999). In contrast to

other bacteria, which possess only the EMP and PP pathways, the cyclic network in pseudomonads results in various additional connections between metabolic nodes that have yet to be determined. Thus far, the analysis of this type of metabolism cannot be achieved by GC-MS-based flux studies, which appears to be a limitation despite the high relevance of this microbial group in industry and health-related research (Nikel, 2016; Poblete-Castro et al., 2012). In fact, a sophisticated setup using ^{13}C labelling information about intracellular phosphorylated sugars from LC-MS analysis is required (Nikel et al., 2015; Sasnow et al., 2016). Such approaches are, unfortunately, complex, expensive, and experimentally difficult (Wiechert and Nöh, 2013).

Here, we present a completely GC-MS-based workflow that allows us to study the carbon metabolism of pseudomonads in full detail. In addition to considering proteinogenic amino acids, our approach considers labelling of glucose and glucosamine from cellular carbohydrates such as glycogen, peptidoglycan and lipopolysaccharides. These constituents provide the following missing information: the labelling status of glucose6-phosphate (G6P) and fructose6-phosphate (F6P), two intermediates at the heart of the EDEMP cycle that are not accessible from amino acids. In combination with carefully selected tracer substrates, our approach fully resolves the EDEMP cycle and the remaining central carbon metabolism of pseudomonads, as demonstrated for two prominent members of the group: the cell factory *P. putida* KT2440 (Nelson et al., 2002) and the human pathogen *Pseudomonas aeruginosa* PAO1 (Bartell et al., 2017).

2. Materials and methods

2.1. Strains and plasmids

P. putida KT2440 (DSM 6125) and *P. aeruginosa* PAO1 (DSM 2264) were obtained from the German Collection of Microorganisms and Cell Cultures (DSMZ, Braunschweig, Germany). The strains were maintained as cryo stocks in 15% (v/v) glycerol at −80 °C.

2.2. Batch cultivation in shake flasks

P. putida KT2440 was grown at 30 °C in minimal medium, which contained the following per litre: 7.5 g glucose, 2 g (NH$_4$)$_2$SO$_4$, 7.75 g K$_2$HPO$_4$, 4.25 g NaH$_2$PO$_4$·2H$_2$O, 0.1 g MgCl$_2$·6H$_2$O, 10 mg EDTA, 5 mg FeSO$_4$·7H$_2$O, 1 mg CaCl$_2$·2H$_2$O and 1 mL of a trace element stock solution, which contained 2 g ZnSO$_4$·7H$_2$O, 1 g MnCl$_2$·2H$_2$O, 0.4 g CoCl$_2$·6H$_2$O, 0.3 g Na$_2$B$_4$O$_7$, 0.2 g Na$_2$MoO$_4$·2H$_2$O, 0.2 g CuSO$_4$·5H$_2$O, and 0.2 g NiCl$_2$·6H$_2$O per litre. *P. aeruginosa* PAO1 was grown at 37 °C in minimal MOPS medium (LaBauve and Wargo, 2012) supplemented with 3.6 g glucose per litre as the sole carbon source. After mixing all components, the pH value of the minimal medium was adjusted to pH 7.0. Prior to the flux experiments, cells from a cryo stock were grown overnight on an agar plate using minimal medium with 15 g l^{-1} agar (Becton Dickinson, Franklin Lakes, NJ, USA), inoculated into a liquid pre-culture in baffled shake flasks filled to 10% with minimal medium, and incubated on a rotary shaker (230 rpm Multifors, Infors AG, Switzerland). During the exponential growth phase, cells were harvested by centrifugation (5 min, 4 °C, 8.000 × *g*), washed once with fresh medium without glucose and then used as inoculum for the main cultures, i.e., parallel isotopic tracer experiments using three different tracers instead of normal glucose: (i) 99% [1–^{13}C] glucose (Sigma-Aldrich, Steinheim, Germany), (ii) 99% [6–^{13}C] glucose (Omicron Biochemicals, Southbend, IN, USA), and (iii) an equimolar mixture of naturally labelled and 99% [^{13}C$_6$] glucose (Eurisotop, Saarbrücken, Germany). The inoculum for the tracer cultures was chosen to be small so that the initial optical density (OD$_{600}$) was below 0.02 and any interference of non-labelled material from the pre-culture with the subsequent ^{13}C-labelling analysis could be neglected (Wittmann, 2007). All experiments comprised three biological replicates.

2.3. Quantification of cells, substrates and products

The cell concentration was monitored spectrophotometrically at 600 nm (UV-1600 PC, VWR International, Darmstadt, Germany). For the determination of the cell dry mass (CDM), cells were collected on pre-weighed and dried membrane filters (0.2 μm, regenerated cellulose, 47 mm, Sartorius, Germany) using vacuum filtration. Then, the filters were washed with 0.9% NaCl and deionized water and dried at 80 °C until a constant weight was achieved. From the measurements, correlation factors of CDM [g L^{-1}] = 0.54 × OD$_{600}$ and CDM [g L^{-1}] = 0.42 × OD$_{600}$ resulted for *P. putida* and *P. aeruginosa*, respectively. Glucose was quantified enzymatically (R-Biopharm, Darmstadt, Germany). Gluconate and 2-ketogluconate were quantified by high-performance liquid chromatography (HPLC) (Agilent 1260 Infinity Series, Agilent Technologies, Waldbronn, Germany), including separation on an Aminex HPX-87H column (Bio-Rad, Hercules, USA), isocratic elution with 50 mM H$_2$SO$_4$ at 65 °C, a flow rate of 0.5 mL min^{-1}, and UV detection at 210 nm.

2.4. Enzymatic assays

Spectrophotometric measurements of gluconokinase (GnuK, EC 2.7.1.12) and 2-ketogluconate kinase (KguK, EC 2.7.1.13) activity were adapted from previous protocols (Nikel et al., 2015; Phibbs et al., 1974; Tlemcani et al., 2008; Vicente and Canovas, 1973) After collection from the cultures, cell pellets were washed twice with 100 mM Tris-HCl buffer (pH 8.0) and resuspended in 100 mM Tris-HCl (pH 8.0) containing 10 mM 2-mercaptoethanol and 1% (v/v) protease inhibitor solution (Protease Inhibitor Cocktail, Sigma-Aldrich, Taufkirchen, Germany). The resuspended cells were then disrupted in a benchtop homogenizer (Precellys, PeqLab, Erlangen, Germany) using 0.1 mm silica beads (Lysing Matrix B, MP Biomedicals, Santa Ana, CA, USA) and 3 disruption cycles of 30 s each at 6000 s^{-1} with a 1 min incubation on ice between cycles. Cell debris was separated via centrifugation (10 min, 4 °C, 21,100 × *g*). Subsequently, the cytosolic fraction, which contained the soluble kinases of interest, was separated from the membrane fraction via ultracentrifugation (90 min, 4 °C, 100,000 × *g*). The protein concentration in the cytosolic extract was determined using a commercial assay (Pierce BCA Protein Assay Kit, Thermo Fisher, Rockford, IL, USA). Gluconokinase activity was assayed in 1 mL of a reaction mixture containing 50 mM Tris-HCl (pH 8.0), 10 mM MgCl$_2$, 6.5 mM ATP, 5 mM NADP$^+$, 0.6 U 6-phosphogluconate (6PG) dehydrogenase, 10 mM sodium gluconate, and 100 μL cytosolic extract. The specific enzyme activity was determined in μmole per min and milligram total protein from a photometric measurement of NADPH formation (calculated from absorption at 340 nm using an extinction coefficient of 6.22 mM^{-1} cm^{-1}). The activity of 2-ketogluconate kinase was measured photometrically using the coupling of 2-ketogluconate-dependent ADP formation to the activities of externally added pyruvate (PYR) kinase and lactate dehydrogenase, resulting in the oxidation of NADH (340 nm) as a readout (Ornston and Ornston, 1969). Reaction mixtures (1 mL) contained 50 mM Tris-HCl, 100 mM KCl, 10 mM MgCl$_2$, 2.5 mM Na-PEP, 0.5 mM ATP, 0.33 mM KCN, 0.33 mM Na$_2$EDTA, 0.25 mM NADH, 1 U PYR kinase, 2.7 U lactate dehydrogenase, 15 mM 2-ketogluconate hemicalcium salt monohydrate, and 100 μL cytosolic extract. The incubation temperatures were 30 °C (KT2440) and 37 °C (PAO1). Negative controls were conducted without cell extract and substrate, and corrections were made accordingly.

2.5. GC-MS labelling analysis of amino acids

For the analysis of proteinogenic amino acids, cells (2 mg CDM) were collected by centrifugation (5 min, 4 °C, 16,000 × *g*), hydrolysed by incubation in 100 μL 6 M HCl for 24 h at 100 °C, and clarified from cell debris by filtration (0.2 μm, Ultrafree-MC, Merck Millipore, Darmstadt, Germany) (Kohlstedt et al., 2014). Subsequently, the

hydrolysate was dried under a nitrogen flow. The obtained amino acids were dissolved in 50 μL *N,N*-dimethylformamide containing 1% (v/v) pyridine and derivatized at 80 °C for 30 min with 50 μL *N*-methyl-*t*-butyldimethylsilyl-trifluoroacetamide (MBDSTFA, Macherey-Nagel, Düren, Germany) (Wittmann et al., 2002). Mass isotopomer distributions (MIDs) of the *t*-butyldimethylsilyl (TBDMS) amino acids were analysed by GC-MS (Agilent 7890A, Quadrupole Mass Selective Detector 5975C, Agilent Technologies). Prior to MS analysis, analytes (0.2 μL injection volume) were separated on an HP-5MS column (30 m, 250 μm × 0.25 μm, Agilent Technologies) using helium as the carrier gas (1.7 mL min^{-1}) and the following temperature program: 120 °C (0–2 min), 8 °C min^{-1} increase (2–12 min), 10 °C min^{-1} increase (12–24.5 min), and 325 °C (24.5–27 min). Further settings controlled the inlet (250 °C), transfer liner (280 °C), ion source (230 °C), and quadrupole temperature (150 °C). Samples were first measured in scan mode to exclude potential isobaric interference of the sample matrix with ion clusters of interest. Subsequently, selective ion monitoring (SIM) was used to quantify MIDs. Altogether, 17 amino acids yielded ion clusters with clean MIDs, which were considered as inputs for flux estimation: alanine (*m/z* 232, *m/z* 260), glycine (*m/z* 218, *m/z* 246), valine (*m/z* 260, *m/z* 288), leucine (*m/z* 200, *m/z* 274), isoleucine (*m/z* 200, *m/z* 274), proline (*m/z* 258), serine (*m/z* 288, *m/z* 362, *m/z* 390), threonine (*m/z* 376, *m/z* 404), phenylalanine (*m/z* 234, *m/z* 302, *m/z* 336), aspartate (*m/z* 316, *m/z* 390, *m/z* 418), glutamate (*m/z* 330, *m/z* 432), lysine (*m/z* 431), arginine (*m/z* 442), histidine (*m/z* 440), and tyrosine (*m/z* 302, *m/z* 466). These fragments have proven suitable for ^{13}C flux studies of pseudomonads previously (Blank et al., 2008; Ebert et al., 2011; Fuhrer et al., 2005; Nikel et al., 2015; Opperman and Shachar-Hill, 2016; Wierckx et al., 2009). Glutamate and aspartate also reflected the pools of glutamine and asparagine, which underwent deamination during protein hydrolysis. The remaining proteinogenic amino acids (cysteine, methionine, and tryptophan) were not available due to their degradation during hydrolysis (Wittmann, 2007).

2.6. GC-MS labelling analysis of sugars

For the analysis of cellular sugars, cells (5 mg CDM) were pelleted by centrifugation, washed twice in deionized water and hydrolysed in 250 μL 2 M HCl for 2 h at 100 °C (Kiefer et al., 2004). Afterwards, cell debris was removed by filtration (0.2 μm, Ultrafree-MC, Merck Millipore). Subsequently, the hydrolysate was dried under nitrogen. Analytes contained in the dried residue were incubated in 100 μL methoxylamine (2% in pyridine) at 80 °C for 1 h. The obtained *O*-methyl oxime forms of the analytes were silylated at 80 °C for 30 min into trimethylsilyl (TMS) derivatives in a second step using *N,O*-bis-trimethylsilyl-trifluoroacetamide (BSTFA, Macherey-Nagel). The derivatized analytes were quantified by GC-MS (Agilent 7890A, Quadrupole Mass Selective Detector 5975C, Agilent Technologies). In the same way, purified biopolymers (glycogen from oysters, peptidoglycan from *B. subtilis*, and lipopolysaccharides from *P. aeruginosa*, all from Sigma-Aldrich, Taufkirchen, Germany) and pure glucose, glucosamine, *N*-acetyl-glucosamine, and mannose were treated as controls for GC-MS analysis. Prior to MS analysis, the analytes (0.2 μL injection volume) were separated on an HP-5MS column (30 m, 250 μm × 0.25 μm, Agilent Technologies) using helium as the carrier gas (1.7 mL min^{-1}) and the following temperature program: 150 °C (0–3 min), 8 °C min^{-1} increase (2–12 min), 25 °C min^{-1} increase (12–15.8 min), and 325 °C (15.8–19 min). Further settings controlled the inlet (250 °C), transfer liner (280 °C), ion source (230 °C), and quadrupole temperature (150 °C). Again, samples were first measured in scan mode to exclude isobaric interference of the matrix with signals from ion clusters of interest. Subsequently, SIM was used for quantitative analysis. The fragments finally considered for flux estimation are listed in Table 1.

2.7. Metabolic reaction networks

The network of *P. putida* KT2440 (Fig. 1) was taken from recent work (Nikel et al., 2015). It contains the EDEMP cycle in full detail: glucose uptake (v_1), subsequent phosphorylation into G6P (v_2), cytoplasmic G6P oxidation by G6P dehydrogenase (v_{16}), periplasmic glucose oxidation into gluconate (Gnt) (v_3) and further into 2-keto-gluconate (2KG) (v_6), secretion of both acids (v_4, v_7), their phosphorylation into 6PG (v_5) and 2-keto-6-phosphogluconate (2K6PG) (v_8), and reduction of 2K6PG into 6PG (v_9). The network also comprised the ED pathway (v_{10}, v_{11}), an incomplete EMP pathway lacking phosphofructokinase (v_{12} to v_{15}, v_{21} to v_{23}), the PP pathway (v_{17} to v_{20}), reactions around the PYR node (v_{24} to v_{27}), the tricarboxylic acid (TCA) cycle (v_{28} to v_{34}), the glyoxylate shunt (v_{35} to v_{36}), and anabolic pathways from 11 precursors to biomass (indicated as green triangles in Fig. 1). According to previous work, the ATP-dependent phosphoenolpyruvate (PEP) carboxykinase-coding gene *pckA* is a functionless pseudogene; thus, its reaction was not included (Belda et al., 2016). Instead, the PEP carboxylase step was considered reversible, as previous studies have shown that there is a small but significant fraction of PEP originating from oxaloacetate (OAA) (Fuhrer et al., 2005; Chavarría et al., 2012; Sudarsan et al., 2014; Sasnow et al., 2016). The cellular composition of *P. putida* KT2440 was taken from a recent reconciliation study (van Duuren et al., 2013). The complete list of biochemical reactions is given in the supplemental material (Table S1).

The network of *P. aeruginosa* PAO1 was adapted from that of a previous flux study (Berger et al., 2014). To account for most recent discoveries, the network was carefully validated against an updated and expanded genome-scale network reconstruction of *P. aeruginosa* PAO1 in terms of the presence of reactions as well as their stoichiometry and directionality (Bartell et al., 2017). An EDEMP cycle annotated in the genome-scale reconstruction was added accordingly. The network differed from that of *P. putida* KT2440 in two major ways (Belda et al., 2016): (i) *P. aeruginosa* PAO1 possesses a PEP carboxykinase (*pckA*) and (ii) operates a membrane-bound, irreversible malate:quinone oxidoreductase (*mqoA, mqoB*) instead of a soluble, reversible malate dehydrogenase (*mdh*). The chemical composition of *P. aeruginosa* PAO1 cells was taken from a previous analysis (Berger et al., 2014). The full reaction list is provided in the supplemental material (Table S2).

In contrast to a simplified network of pseudomonads with a lumped glucose metabolism (Sudarsan et al., 2014), the fully detailed network with the EDEMP cycle included four additional free flux parameters (Eqs. (1)–(4)): the flux partitioning ratios at the periplasmic nodes of (i) glucose (Φ_{Glc}) and (ii) gluconate (Φ_{Gnt}) and at the cytosolic nodes of (iii) 6PG (Φ_{6PG}) and (iv) glyceraldehyde3-phosphate (G3P) (Φ_{G3P}) (Fig. 1).

$$\Phi_{Glc} = \frac{v_2}{v_2 + v_3} \tag{1}$$

$$\Phi_{Gnt} = \frac{v_8}{v_5 + v_8} \tag{2}$$

$$\Phi_{6PG} = \frac{v_{17}}{v_{10} + v_{17}} \tag{3}$$

$$\Phi_{G3P} = \frac{v_{12}}{v_{12} + v_{21}} \tag{4}$$

The two branches at the periplasmic gluconate node, whose reactions are catalyzed by gluconokinase (v_5) and 2-ketogluconate kinase (v_8), possess identical stoichiometry and carbon atom transitions, excluding their discrimination by steady-state ^{13}C MFA (Fig. 1). Accordingly, the flux partitioning ratio at the gluconate node (Φ_{Gnt}) was inferred from activity measurements of the two key enzymes involved, as done previously (Nikel et al., 2015; Tlemcani et al., 2008). The identifiability of the other flux parameters of the EDEMP cycle by ^{13}C-labelling data was investigated in this work (see below).

Table 1

GC-MS analysis of glucose and glucosamine in hydrolysed biomass of *Pseudomonas putida* KT2440. Sugars were analysed as TMS-methoxime derivatives. For comparison, data from the analysis of pure standards (glucose, glucosamine) and hydrolysed polymers (glycogen, peptidoglycan) are shown. In addition, the theoretical mass isotopomer distribution for each fragment is given. The monoisotopic mass is denoted m + 0, while m + 1 and m + 2 indicate mass isotopomers of higher mass. The labelling pattern of the glucose fragment at *m/z 160*, highlighted in dark grey, differed from the theoretical expectations, so it was not considered further. n = 3.

				Glucose		
Fragment	**Mass**	***m/z***	**Theoretical value**	**Glucose standard**	**Hydrolysed glycogen**	**Hydrolysed biomass**
$[C_1 - C_6]$	m+0	*554.4*	0.521	0.521 ± 0.002	0.521 ± 0.002	0.522 ± 0.002
	m+1	*555.4*	0.258	0.258 ± 0.002	0.258 ± 0.002	0.257 ± 0.002
	m+2	*556.4*	0.154	0.153 ± 0.002	0.151 ± 0.003	0.150 ± 0.003
$[C_3 - C_6]$	m+0	*319.2*	0.675	0.673 ± 0.002	0.672 ± 0.003	0.673 ± 0.003
	m+1	*320.2*	0.202	0.202 ± 0.003	0.203 ± 0.003	0.202 ± 0.002
	m+2	*321.2*	0.099	0.099 ± 0.003	0.099 ± 0.002	0.098 ± 0.003
$[C_1 - C_2]$	m+0	*160.1*	0.857	0.816 ± 0.002	0.816 ± 0.004	0.816 ± 0.003
	m+1	*161.1*	0.105	0.142 ± 0.003	0.142 ± 0.003	0.142 ± 0.003

				Glucosamine		
Fragment	**Mass**	***m/z***	**Theoretical value**	**Glucosamine standard**	**Hydrolysed peptidoglycan**	**Hydrolysed biomass**
$[C_1 - C_6]$	m+0	*553.4*	0.520	0.521 ± 0.002	0.523 ± 0.002	0.523 ± 0.002
	m+1	*554.4*	0.259	0.258 ± 0.002	0.258 ± 0.002	0.258 ± 0.002
	m+2	*555.4*	0.153	0.153 ± 0.002	0.150 ± 0.003	0.150 ± 0.003
$[C_3 - C_6]$	m+0	*319.2*	0.675	0.675 ± 0.002	0.674 ± 0.002	0.675 ± 0.003
	m+1	*320.2*	0.202	0.202 ± 0.002	0.203 ± 0.003	0.202 ± 0.002
	m+2	*321.2*	0.099	0.100 ± 0.002	0.098 ± 0.003	0.098 ± 0.003
$[C_1 - C_2]$	m+0	*159.1*	0.856	0.854 ± 0.002	0.852 ± 0.004	0.855 ± 0.004
	m+1	*160.1*	0.107	0.109 ± 0.003	0.111 ± 0.003	0.109 ± 0.003

In addition, free fluxes around the TCA cycle (Eqs. (5)–(7)) were included and tested in the simulations: the flux partitioning ratios at the cytoplasmic nodes of (i) PYR (Φ_{PYR}), (ii) OAA (Φ_{OAA}), and (iii) isocitrate (ICT) (Φ_{ICT}) (Fig. 1).

$$\Phi_{PYR} = \frac{v_{25}}{v_{24} + v_{25}} \tag{5}$$

$$\Phi_{OAA} = \frac{v_{26}}{v_{26} + v_{28}} \tag{6}$$

$$\Phi_{ICT} = \frac{v_{35}}{v_{30} + v_{35}} \tag{7}$$

2.8. Computational design of flux experiments: sensitivity analysis

Model-based design of flux experiments was performed using OpenFLUX (Quek et al., 2009). For this purpose, the metabolic reaction networks were implemented with their corresponding carbon transformations into the software. To enable simulations with parallel labelling data sets, a recently developed, extended version of OpenFLUX was used (Lange et al., 2017).

In the first stage, the suitability of different tracer substrates for the estimation of flux parameters was studied by sensitivity analysis (Wittmann and Heinzle, 2001b). In a series of simulations, individual flux parameters were varied while the other fluxes in the network were kept constant (Nikel et al., 2015), and the effect of the flux variation on

^{13}C-labelling data was studied. This procedure unravelled (sensitive and therefore) potentially suitable tracers and analyte fragments for a given flux analysis problem.

2.9. Metabolic flux calculation and statistical evaluation

Flux calculations were performed using OpenFLUX (Quek et al., 2009). To handle parallel labelling data sets, the extended version of OpenFLUX was used (Lange et al., 2017). Quantitative estimation of intracellular fluxes utilized ^{13}C-labelling data and directly measured fluxes. Experimental MIDs were automatically corrected for the natural abundance of isotopes (van Winden et al., 2002) using an algorithm in OpenFLUX (Quek et al., 2009) and a measurement error of 0.3 mol% for the GC-MS measurements (Long et al., 2016; Quek and Nielsen, 2014). The metabolic model was constrained (Quek and Nielsen, 2014) with measured secretion rates for gluconate and 2-ketogluconate (Table 2) and anabolic fluxes into biomass (Table 3) that were inferred from cell composition and measured biomass yields (Table 2). Lower and upper bounds for these fluxes were defined using the preSolver function of OpenFLUX (Lehnen et al., 2017). The set of free fluxes that resulted in the minimum deviation between the experimental and simulated labelling data was taken as the best estimate for the *in vivo* fluxes (Wittmann and Heinzle, 2002). Fragments were inspected for the quality of fit to eventually identify unsuitable signals. Because the nonlinear structure of isotopomer models may potentially lead to local

Table 2

Kinetics and stoichiometry of glucose-grown *Pseudomonas putida* KT2440 and *Pseudomonas aeruginosa* PAO1. The data comprise specific rates for growth (μ_{max}), glucose uptake (q_{Glc}), gluconate formation (q_{Gnt}), and 2-ketogluconate formation (q_{2KG}). In addition, the yields for biomass ($Y_{X/Glc}$), gluconate ($Y_{Gnt/Glc}$) and 2-ketogluconate ($Y_{2KG/Glc}$) are displayed. n = 3.

Strain	μ_{max} [h^{-1}]	q_{Glc} [mmol g^{-1} h^{-1}]	q_{Gnt} [mmol g^{-1} h^{-1}]	q_{2KG} [mmol g^{-1} h^{-1}]	$Y_{X/Glc}$ [g mol^{-1}]	$Y_{Gnt/Glc}$ [mol mol^{-1}]	$Y_{2KG/Glc}$ [mol mol^{-1}]
KT2440	0.55 ± 0.02	6.8 ± 0.2	0.6 ± 0.0	0.1 ± 0.0	81.6 ± 7.8	0.09 ± 0.02	0.02 ± 0.00
PAO1	0.90 ± 0.02	9.7 ± 0.2	0.2 ± 0.1	0.2 ± 0.0	92.6 ± 2.6	0.03 ± 0.01	0.03 ± 0.02

Table 3
Anabolic precursor demand of glucose-grown *Pseudomonas putida* KT2440 and *Pseudomonas aeruginosa* PAO1. The data are derived from biomass yield (Table 2) and the cellular composition of each strain and are given in mmol (mol glucose)$^{-1}$. Normalized to the glucose uptake rate (100%), the demand equals the relative anabolic flux in the corresponding flux maps (Figs. 6 and 7). The relative anabolic fluxes (%) can be obtained by dividing the values given in the table by a factor of 10. n = 3.

| Precursor	KT2440	PAO1
G6P	14.2 ± 1.4	19.0 ± 0.4
F6P	5.6 ± 0.6	6.6 ± 0.1
R5P	54.7 ± 0.5	83.2 ± 1.8
E4P	27.7 ± 0.3	33.4 ± 0.7
G3P	8.8 ± 0.9	11.9 ± 0.3
3PG	88.6 ± 8.9	138.3 ± 3.1
PEP	58.4 ± 5.8	66.6 ± 1.5
PYR	143.5 ± 14.3	262.3 ± 5.8
AcCoA	204.9 ± 20.5	271.1 ± 6.0
AKG	78.3 ± 7.8	97.2 ± 2.2
OAA	110.4 ± 11.0	165.5 ± 3.7

minima, multiple parameter initialization (250 simulations per strain) with randomly chosen starting values was used to investigate whether the obtained flux distribution represented the global optimum. Statistical analysis of the obtained fluxes was conducted by Monte-Carlo analysis and yielded 95% confidence intervals for the flux parameters (Becker et al., 2005).

2.10. Computational evaluation of flux experiments: flux identifiability, precision and accuracy

Different setups were evaluated for their capability to successfully assess the flux distribution, which was determined in this study for *P. putida* KT2440 and *P. aeruginosa* PAO1 from all available data, i.e., values of 534 mass isotopomers from three parallel experiments (see below). The test setups included different sets of labelling data from single-tracer studies, double-tracer studies on two different combinations of tracers and a complete data set from a triple study on all three different tracers. The evaluation was conducted by Monte-Carlo analysis. For each setup, the labelling data were (i) randomly varied within the experimental noise and then (ii) used as input in repeated flux estimations to investigate the capability of these estimations to re-determine the flux values. In this regard, such a Monte-Carlo analysis mimicked 25 repetitions of the same flux experiment while taking experimental errors into account, and in this way, it allowed the overall precision and accuracy expected from this particular setup to be studied. In addition, a precision score (ϑ) that summarized the deviation of the fluxes from the optimum values for each setup was calculated (Eq. (8)).

$$\vartheta = \sum_{1}^{i} \sum_{1}^{j} \frac{1}{|v_j - v_{j,opt}|} \tag{8}$$

For this purpose, the deviation of all net fluxes (v_j) in the network (j = 44) from their corresponding optimum values ($v_{j,\ opt}$) was summed for all flux distributions (i = 25) obtained by the Monte-Carlo analysis. The use of the reciprocal value turned the total deviation into a precision score. For comparison, precision scores were given as relative values normalized to the highest precision score obtained, i.e., that of the best setup.
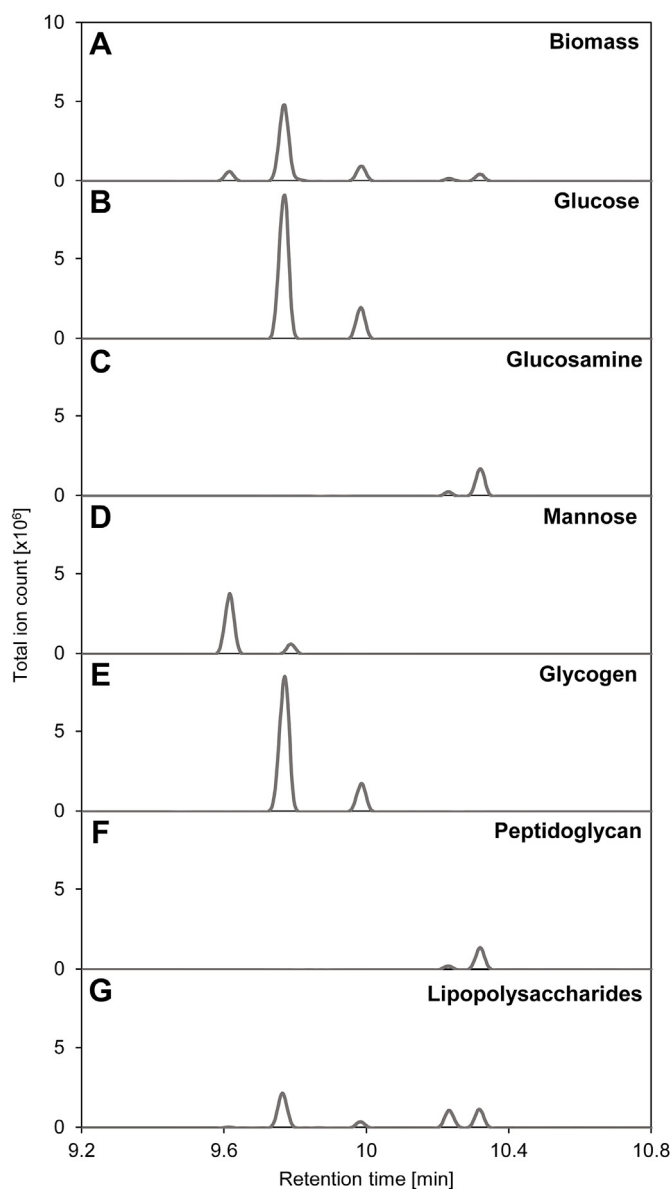
Fig. 2. GC-MS analysis of glucose and glucosamine monomers in biomass hydrolysates of *Pseudomonas putida* KT2440. In addition to biomass (A), the data show total ion current (TIC) chromatograms of glucose (B), glucosamine (C), mannose (D), hydrolysed glycogen (E), hydrolysed peptidoglycan (F), and hydrolysed lipopolysaccharides (G). All compounds were analysed as methyloxime-trimethylsilyl derivatives after two-step derivatization with methoxylamine and *N,O*-bis-trimethylsilyl-trifluoroacetamide (BSTFA).

3. Results

3.1. GC-MS analysis of glucose and glucosamine from hydrolysed cell carbohydrates provides direct access to the ^{13}C-labelling pattern of G6P and F6P

First, we identified biomass-derived metabolites in *P. putida* KT2440, which could provide useful labelling information for flux resolution. *P. putida* cells grown on naturally labelled glucose were harvested and subjected to mild hydrolysis. After a two-step derivatization, the obtained biomass hydrolysate was analysed by GC-MS. Its total ion chromatogram showed several prominent signals (Fig. 2A). Comparing the elution time and mass spectra of this sample with those of pure standards revealed that the hydrolysate contained significant amounts of glucose and glucosamine and a minor share of mannose (Fig. 2 BCD).
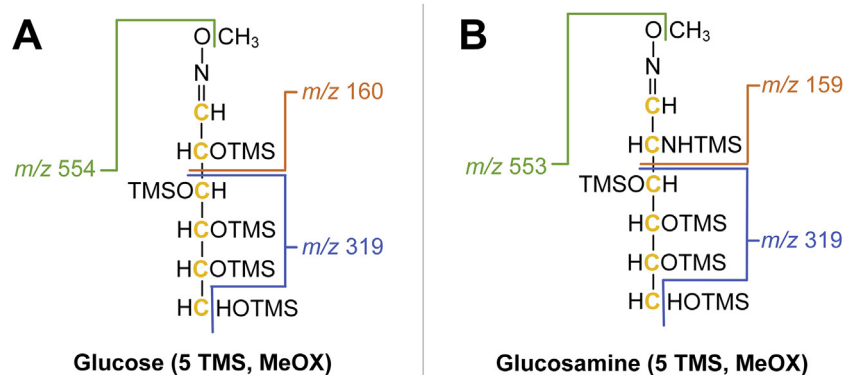
Fig. 3. Chemical structure of glucose (A) and glucosamine (B) after two-step derivatization with methoxylamine and *N,O*-bis-trimethylsilyl-tri-fluoroacetamide (BSTFA). The structure of prominent analyte fragments formed during GC-MS analysis is also displayed.

Additional studies with pre-purified cellular polymers revealed that glucose in the biomass originated from glycogen and lipopolysaccharides (Fig. 2 EG). Cellular glucosamine could be related to peptidoglycan and lipopolysaccharides (Fig. 2 FG) and typically occurs as an *N*-acetyl-glucosamine derivative in these polymers (Michal, 1999). Additional studies revealed that *N*-acetyl-glucosamine underwent deacetylation to glucosamine during hydrolysis, explaining the presence of the latter in the analysis. Mannose was found to a low extent in the lipopoly-saccharides (Fig. 2 G). Each compound resulted in two peaks due to the occurrence of *syn* and *anti* isomers.

Then, assessing whether the signals contained unbiased labelling patterns of the sugars was interesting. The second peak of glucose (at 10 min) was used to extract mass spectra to avoid potential interference with signals from mannose. Two prominent ion cluster mass spectra represented a C_1–C_6 fragment (m/z 554–560) and a C_3–C_6 fragment (m/z 319–323) of glucose (Fig. 3A). The MIDs of both clusters from the biomass sample were identical to that of a glucose standard and that of glucose obtained from hydrolysed glycogen (Table 1). Furthermore, all values showed excellent agreement with the theoretical MIDs of the derivatized sugar fragments inferred from the natural abundance of isotopes (van Winden et al., 2002). The labelling pattern of the glucose fragment at m/z 160–162, however, differed from the expected pattern, obviously due to isobaric interference with the sample matrix, and was therefore not considered further (Table 1). Cellular glucosamine yielded three fragments with clean spectra: a C_1–C_6 fragment at m/z 553–559, a C_3–C_6 fragment at m/z 319–323, and a C_1–C_2 fragment at m/z 159–161 (Fig. 3B). The MIDs of all three fragments in the biomass hydrolysate matched those of a pure glucosamine standard, cellular peptidoglycan and theoretical MIDs (Table 1). Biomass samples taken from *P. aeruginosa* PAO1 provided access to the same fragments and exhibited equal analytical quality. In metabolism, glucose and glucosamine in biomass each have one exclusive metabolic precursor: G6P (glucose) and F6P (glucosamine), respectively (Michal, 1999). Accordingly, the analytical approach accurately provided the labelling patterns of G6P and F6P. This discovery appeared promising because G6P and F6P are central hubs of the EDEMP cycle, and neither is accessible in ^{13}C labelling via analysis of the proteinogenic amino acids (Wittmann, 2007). Mannose, also potentially accessible, was not considered further. Its signals were generally weaker, and since it is also formed from F6P, it would not have added novel information to the data set.

3.2. Cellular carbohydrate sugars provide sensitive ^{13}C-labelling information for inferring EDEMP cycle fluxes
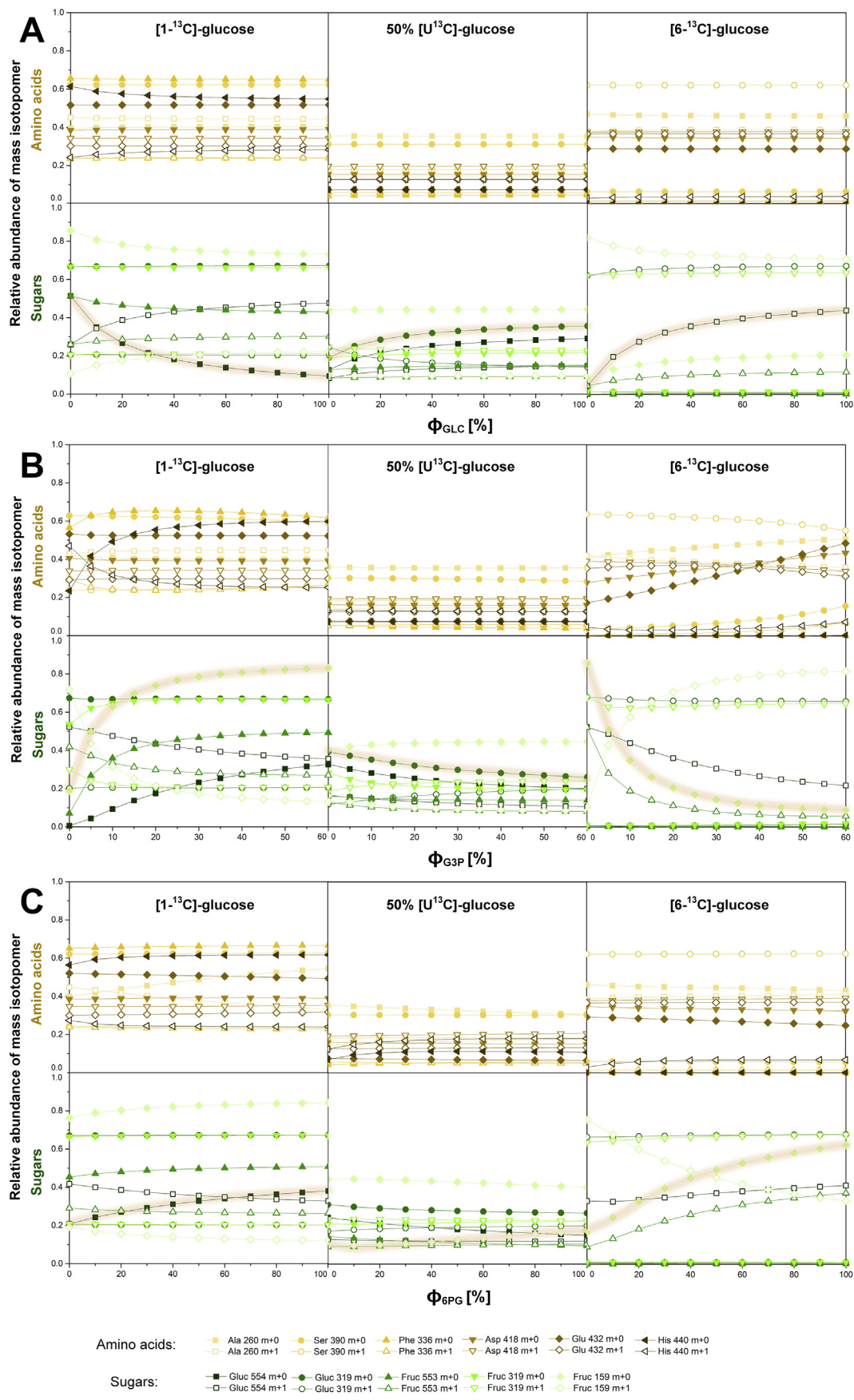
In a series of simulations, the sensitivity of the estimation of the EDEMP cycle fluxes to the labelling data (amino acids plus sugars) was systematically studied. In each run, one flux parameter of interest was varied while the other free fluxes were kept constant. The tested tracers comprised the most widely used, commercially available variants: $[1-^{13}C]$, $[2-^{13}C]$, $[3-^{13}C]$, $[4-^{13}C]$, $[5-^{13}C]$, and $[6-^{13}C]$ glucose plus an equimolar mixture of $[^{13}C_6]$ and naturally labelled glucose. First, the Φ_{Glc} was varied between 0% (exclusive oxidation into periplasmic gluconate) and 100% (exclusive phosphorylation into cytosolic G6P). The labelling pattern of different fragments of glucose and glucosamine significantly changed upon the flux variation. This effect was prominent for $[1-^{13}C]$ glucose, $[6-^{13}C]$ glucose, and the mixture of $[^{13}C_6]$ and non-labelled glucose (Fig. 4A) and occurred for other tracers (Fig. S3). Similarly, the two sugar derivatives reflected changes in Φ_{6PG}, and Φ_{G3P}, the other free flux partitioning ratios of the EDEMP cycle (Fig. 4 BC and S3). The sensitivity was generally high. For example, the non-labelled fraction of derivatized glucosamine (m/z 159) increased by more than 400% over the tested Φ_{G3P} range. The specific changes in labelling for each flux parameter tested appeared beneficial. For example, a variation in Φ_{Glc} for the $[6-^{13}C]$ tracer changed the labelling in the cellular glucose pool (Fig. 4A), whereas that in the glucosamine pool did not change. Changes in Φ_{6PG} had the opposite effect on the same tracer: glucosamine labelling responded, but glucose labelling did not (Fig. 4C). Accordingly, the sugars, i.e., the two pools G6P and F6P delivered complementary labelling information.

In contrast, the labelling status of proteinogenic amino acids remained relatively constant and independent of the type of tracer applied when the EDEMP fluxes were varied (Figs. 4A and S3). The glucose split (Φ_{Glc}) had practically no sensitivity. Weak sensitivity to histidine and glutamate (and to a lower extent aspartate and threonine) was found for triose recycling (Φ_{G3P}) and the 6PG split (Φ_{6PG}). Taking these results together, the newly introduced sugars appeared particularly valuable for accessing EDEMP cycle fluxes. In contrast, the amino acid patterns alone seemed insufficient to fully resolve this part of the network. However, the resolution of fluxes at important branch points of the lower carbon metabolism was substantially sensitive to amino acids (Fig. S4).

3.3. The novel approach provides metabolic fluxes in P. putida KT2440 at high resolution and high accuracy

Three parallel labelling experiments, one on $[1-^{13}C]$ glucose, one on $[6-^{13}C]$ glucose, and one on a mixture of $[^{13}C_6]$ and non-labelled glucose, were conducted for *P. putida* KT2440. The cells consumed glucose at a specific rate of $6.8 \, \text{mmol g}^{-1} \, \text{h}^{-1}$ and formed small amounts of gluconate and 2-ketogluconate as by-products in addition to biomass (Table 2). The two enzymes of the gluconate by-pass and the 2-ketogluconate loop, i.e., gluconokinase and 2-ketogluconate kinase, were both expressed, and they exhibited an activity ratio of 20:1 (Table 4). MFA, as applied here, requires a metabolic and isotopic steady state of the investigated culture (Becker et al., 2008). Both were ensured from further analysis of the cultures, i.e., a metabolic steady state was

Amino acids:
- Ala 260 m+0
- Ala 260 m+1
- Ser 390 m+0
- Ser 390 m+1
- Phe 336 m+0
- Phe 336 m+1
- Asp 418 m+0
- Asp 418 m+1
- Glu 432 m+0
- Glu 432 m+1
- His 440 m+0
- His 440 m+1

Sugars:
- Gluc 554 m+0
- Gluc 554 m+1
- Gluc 319 m+0
- Gluc 319 m+1
- Fruc 553 m+0
- Fruc 553 m+1
- Fruc 319 m+0
- Fruc 319 m+1
- Fruc 159 m+0
- Fruc 159 m+1

(caption on next page)

Fig. 4. Computational design of labelling experiments for ^{13}C metabolic flux analysis of *P. putida* KT2440 and *P. aeruginosa* PAO1. The data show the sensitivity of mass isotopomer distributions of amino acids and sugars from hydrolysed cells accessible by GC-MS analysis towards flux changes at key branch points of the EDEMP cycle: Φ_{Glc} (at the periplasmic glucose pool) (A), Φ_{G3P} (at the cytoplasmic G3P pool) (B), and Φ_{6PG} (at the cytoplasmic 6PG pool) (C). In each scenario, one flux parameter of interest was varied while the other fluxes in the network were kept constant. The results display the simulations on $[1-^{13}C]$, $[6-^{13}C]$, and a $[^{13}C_6]$ and naturally labelled glucose mixture. The results for $[2-^{13}C]$, $[3-^{13}C]$, $[4-^{13}C]$, and $[5-^{13}C]$ glucose are given in the supplemental material (Fig. S3).

Table 4

Activity of gluconokinase and 2-ketogluconate kinase in glucose-grown *Pseudomonas putida* KT2440 and *Pseudomonas aeruginosa* PAO1.

Enzyme activity	KT2440	PAO1
Gluconokinase [mU mg^{-1}]	85.0 ± 3.2	193.1 ± 22.4
2-Ketogluconate kinase [mU mg^{-1}]	4.2 ± 1.4	10.8 ± 1.9
Enzyme activity ratio	20.3 ± 7.1	17.8 ± 3.8

ensured by constant growth and production behaviour (Fig. S1), and an isotopic steady state was ensured by constant ^{13}C-labelling patterns over time (Fig. S2). A labelling analysis of all three isotope experiments provided 534 mass isotopomers to be explored (Table S3). The corresponding flux calculation, which considered all data, was carried out by minimizing the deviation between the experimental and calculated mass isotopomer fractions. Identical flux distributions were obtained in 250 estimations with randomly varied starting values for the free fluxes, which showed that the acquired data were indeed fully descriptive and that the determined flux distribution displayed the global flux minimum. Furthermore, excellent agreement between experimentally determined and calculated mass isotopomer ratios was achieved (Fig. 5A, Table S3).

The approach delivered the full flux distribution for *P. putida* KT2440 and precisely determined all fine structures of the network (Fig. 6). The microbe operated the entire EDEMP cycle and revealed a pronounced periplasmic metabolism. Only 33% of glucose entered the central glycolytic routes via direct phosphorylation. The major fraction of glucose was oxidized into gluconate, which was then phosphorylated into 6PG. The by-pass via 2-ketogluconate (2KG) and 2K6PG carried a small but significant flux. Furthermore, 6PG was mainly channelled into the ED pathway (108%). A small but significant flux (2%) supplied carbon into the PP pathway via 6PG dehydrogenase and generated NADPH. The cells recycled G3P back to F6P and G6P, which completed the EDEMP cycle and contributed to the formation of erythrose4-phosphate (E4P) and ribose5-phosphate (R5P) for anabolism via the reversible steps of the PP pathway. The major fraction of G3P was

channelled downstream of the EMP pathway, where it merged with the ED pathway flux at the PYR node. In addition, *P. putida* operated a highly active TCA cycle, whereas the glyoxylate shunt was inactive. The concerted action of malic enzyme, PYR carboxylase, and PEP carboxylase formed another cyclic pathway. Thus, the contribution of malic enzymes was particularly high. The enzyme supplied almost one-quarter of the total influx into the PYR pool. Statistical evaluation revealed that fluxes were determined at high precision (Fig. 6).

3.4. The glucose metabolism in P. aeruginosa PAO1 is dominated by strong periplasmic glucose oxidation and involves the EDEMP cycle

The fluxes of *P. aeruginosa* PAO1 were analysed by the same approach. Slight amounts of gluconate and 2KG were secreted, while the cells consumed glucose at a high uptake rate of almost 10 mmol g^{-1} h^{-1} (Table 2). Gluconokinase was approximately 18-fold more active than 2-ketogluconate kinase (Table 4). The microbe exhibited a metabolic (Fig. S1B) and an isotopic steady state (Fig. S2B) as *P. putida* KT2440 did. GC-MS labelling analysis again provided 534 accurate mass isotopomer fractions (Table S3), which delivered identical flux estimates in 250 independent runs with varied initialization values and yielded an excellent fit (Fig. 5B, Table S3). The microbe used the full EDEMP cycle (Fig. 7), and its periplasmic metabolism was the dominant route for the catabolization of glucose. The fraction of glucose oxidized into gluconate in the periplasm was even 20% higher than that in *P. putida* KT2440. The alternative route of glucose metabolization via G6P was relatively weak (14%). Periplasmic gluconate and 2KG, formed from glucose through oxidation, were largely kept inside of the cells and merged downstream at the 6PG pool. Only a small fraction of the compounds was excreted.

Interestingly, zero flux was measured through 6PG dehydrogenase at the entry into the PP pathway. In fact, 6PG was completely channelled into the ED pathway. The absence of flux through 6PG dehydrogenase resulted in the exclusive supply of E4P and R5P via the recycling of triose units so that the EDEMP cycle appeared essential for growth. The upper glycolysis operated in the gluconeogenic direction.
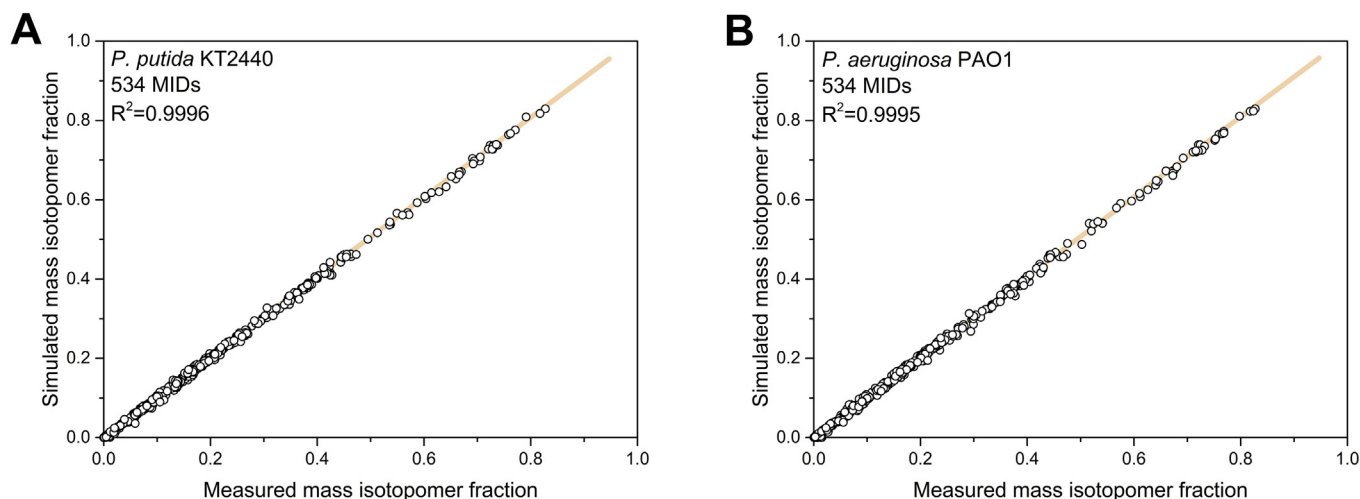
Fig. 5. Goodness of fit for ^{13}C metabolic flux analysis of *Pseudomonas putida* KT2440 (A) and *Pseudomonas aeruginosa* PAO1 (B). The data show the correlation between the abundances of 534 mass isotopomers of amino acids and sugars experimentally measured by GC-MS and the corresponding simulated values, which reflected the optimum fit and the global minimum in the flux estimation. The experimental data for each strain were collected from three parallel tracer experiments ($[1-^{13}C]$, $[6-^{13}C]$, and a 1:1 mixture of $[^{13}C_6]$ plus naturally labelled glucose) (Table S3).
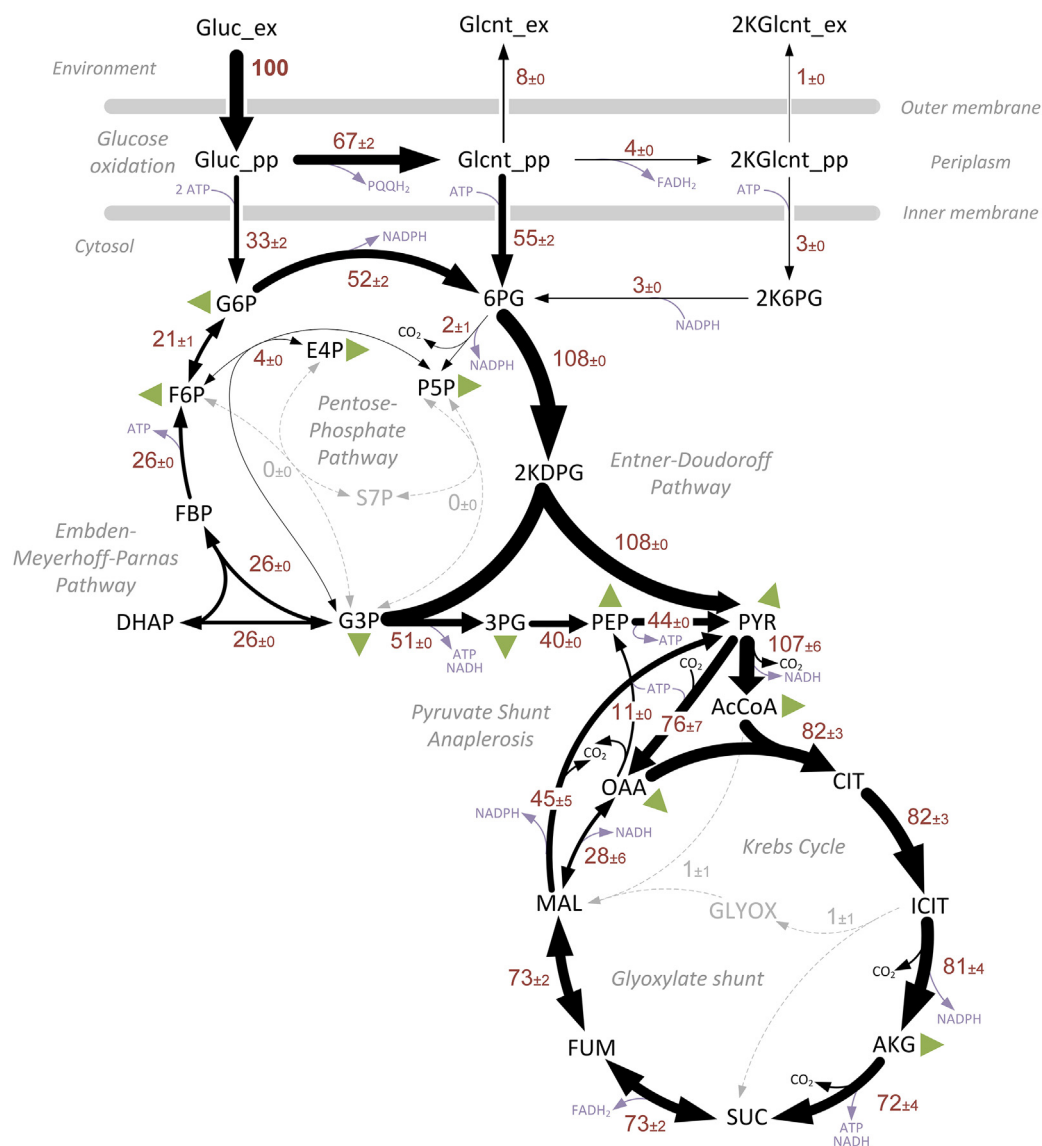
Fig. 6. Intracellular carbon fluxes of glucose-grown *Pseudomonas putida* KT2440 as determined by ^{13}C metabolic flux analysis. All fluxes are given as a molar percentage of the mean specific glucose uptake rate of $q_{Glc} = 6.8 \, \text{mmol} \, \text{g}^{-1} \, \text{h}^{-1}$, which was set to 100%. Reactions generating biomass are indicated as green triangles. Their flux values are not shown here but can be inferred from Table 3. (For interpretation of the references to colour in this figure legend, the reader is referred to the Web version of this article.)

At the level of G6P, approximately half of the carbon resulted from the recycling pathway. In contrast to *P. putida, P. aeruginosa* PAO1 utilized the glyoxylate shunt. Approximately 6% of the flux was directed into this pathway, while the remaining flux at the isocitrate node (72%) was converted by isocitrate dehydrogenase through the TCA cycle. The fluxes between the EMP pathway and the TCA cycle were substantial, and large amounts of C_3 and C_4 building blocks were exchanged between the pathways. The differences between the two microbes were pronounced in terms of absolute flux and related to the growth and glucose uptake of *P. aeruginosa* PAO1 being much faster than that of *P. putida*. The absolute flux through the periplasmic glucose pathway was twice as high in the *P. aeruginosa* strain (8.2 mmol g^{-1} h^{-1}) than in *P. putida* KT2440 (4.1 mmol g^{-1} h^{-1}). Likewise, the ED pathway and the TCA cycle carried 50% more absolute flux.

3.5. Computational analysis reveals that cellular carbohydrates are crucial for accurate flux estimation

As demonstrated, the combined data set of amino acid and sugar labelling from the three parallel tracer experiments enabled a precise and accurate estimation of flux (Figs. 6 and 7). We then evaluated the developed approach in more detail and compared it to different alternative groupings of data. In particular, we were interested in answering the following important questions: Is the labelling of glucose and glucosamine required for successful flux analysis in pseudomonads or would the labelling patterns of the amino acids alone be sufficient? Is a set of three parallel tracer studies truly needed to resolve the fluxes or would fewer experiments suffice?

For this purpose, we used a Monte-Carlo approach. Put simply, this approach allowed the simulation of twenty-five repetitions of a particular flux experiment while network details and experimental errors were fully considered. The outcome of such a simulation was 25 realistic flux distributions. An inspection of these flux distributions then showed how precisely individual flux values, e.g., ratios at branch points, were determinable by the given flux experiment, i.e., a specific tracer and labelling data set. Performing these simulations and inspections for different setups, i.e., different tracers and different labelling data sets, allowed comparison (Fig. 8). We compared different

Fig. 7. Intracellular carbon fluxes of glucose-grown *Pseudomonas aeruginosa* PAO1 as determined by ^{13}C metabolic flux analysis. All fluxes are given as a molar percentage of the mean specific glucose uptake rate of q_{Glc} = 9.7 mmol g^{-1} h^{-1}, which was set to 100%. The reactions generating biomass are indicated as green triangles. Their flux values are not shown here but can be taken from Table 3. (For interpretation of the references to colour in this figure legend, the reader is referred to the Web version of this article.)

tracer combinations (shown in rows A – G) and labelling data sets (columns I – IV). We then visualized the suitability of a particular setup by its capability to estimate key branch points in upper carbon metabolism (around the EDEMP cycle) and lower carbon metabolism (PYR node, TCA cycle, and glyoxylate shunt). The data shown in Fig. 8 and presented below refer to *P. putida* KT2440, but notably, the outcome was the same for *P. aeruginosa* PAO1 (see supplemental material, Fig. S5).

The numbers of parallel studies, the choice of the tracer and the type of labelling had strong effects on the quality of the flux estimation. Most importantly, the information from glucose and glucosamine labelling was crucial to accurately determine the EDEMP cycle fluxes (Fig. 8 A-II, C-II, and D-II). In contrast, none of the scenarios that considered only amino acid labelling appeared suitable (Fig. 8, column I). Most cases resulted in unresolvable fluxes, as indicated by the substantial scattering of solutions from repeated experiments (Fig. 8 E-I, F-I, and G-I). In other cases, the flux values grouped more closely together. At first glance, this behaviour indicated apparently better precision, but the solutions were inaccurate and sometimes far away from the correct flux values (Fig. 8 B-I and C-I). This problem was even observed when amino

acids involving all three tracers were considered (Fig. 8 A-I). Likewise, key branch points in the lower carbon metabolism could not be exactly determined from the amino acid labelling information alone (Fig. 8, column III). In contrast, the additional consideration of the sugar-based labelling data gave completely different results and allowed a precise and accurate quantification of the fluxes (Fig. 8 A-II, and A-IV).

3.6. Precision scoring highlights the most suitable setups for flux analysis

To make a quantitative comparison, the obtained simulation results for *P. putida* KT2440 and *P. aeruginosa* PAO1 were converted into precision scores (Fig. 9) that represented a quantitative measure of the precision of a particular setup in determining the fluxes. The results clearly showed that for both microbes, the highest precision was by far most clearly observed for the triple tracer combination, i.e., parallel studies on [1–^{13}C], [6–^{13}C], and an equimolar mixture of [^{13}C$_6$] and naturally labelled glucose, and the consideration of amino acids and sugars. With regard to practicality, this approach appeared as the only suitable setup. Lower precision, i.e., a relative score between 20 and 50%, resulted from the two double tracer combinations with amino

(caption on next page)

Fig. 8. Computational evaluation of different setups for GC-MS-based ^{13}C metabolic flux analysis of *P. putida* KT2440. The aim of the simulations was to identify optimum strategies for flux analysis in the microbe. Different setups were analysed for their flux precision and accuracy. Key fluxes of upper and lower carbon metabolism, i.e., the flux partitioning ratios in the EDEMP cycle (Φ_{Glc}, Φ_{6PG}, Φ_{G3P}) and around the pyruvate node and the TCA cycle (Φ_{PYR}, Φ_{OAA}, Φ_{ICT}) were thereby taken as indicators. Each setup was evaluated by a Monte-Carlo approach that mimicked 25 repetitions of the corresponding flux study while taking experimental errors into account. The investigated cases included setups with three parallel tracer experiments ([1–^{13}C] glucose, [6–^{13}C] glucose, and a mixture of [[13]C$_6$] and naturally labelled glucose) (A), two parallel experiments on two different tracers (B, C, D), and one single-tracer experiment (E, F, G). Moreover, different metabolites were tested as experimental inputs, i.e., amino acid labelling patterns alone (columns I and III) and amino acid plus sugar labelling patterns (columns II and IV). The outcome (and suitability) of each test case is visualized as follows. The individual fluxes from the 25 Monte-Carlo estimations are given as small green balls. In addition, their mean value is shown as a small red ball. Furthermore, the correct (optimum) flux values obtained from the full approach are shown as large purple balls. The corresponding data for *P. aeruginosa* are given in the supplemental material (Fig. S5). (For interpretation of the references to colour in this figure legend, the reader is referred to the Web version of this article.)

acids and sugars, which included one experiment with [6–^{13}C] glucose. All other scenarios failed to provide satisfying precision, as indicated by their low scores.

4. Discussion

4.1. The developed approach enables GC-MS-based metabolic flux analysis of pseudomonads with high resolution and accuracy

Without doubt, ^{13}C MFA is a key technology in metabolic engineering and industrial biotechnology (Schwechheimer et al., 2018), and it has also greatly contributed to systems biology studies of medically (Beste et al., 2011; Bücker et al., 2014) and environmentally relevant microbes (Tang et al., 2007, 2009).

As shown, our approach enables high-resolution flux analysis of *P. putida* KT2440 and *P. aeruginosa* PAO1 from GC-MS cell constituent data (Figs. 6 and 7). The key to success is the additional analysis of

glucose (G6P) formed from glycogen and lipopolysaccharides and of glucosamine (F6P) formed from peptidoglycan and lipopolysaccharides. These two analytes provide complementary information that is accessible from neither one of them alone nor from amino acids, and combining their assessment with that of amino acids is crucial to resolving the flux network of the microbes in this study (Figs. 4 and 8). As shown, the combination of three tracers, i.e., [1–^{13}C], [6–^{13}C] and 50% [[13]C$_6$] glucose, in parallel cultures provides maximum accuracy and precision and seems a method of choice for highly quantitative studies (Fig. 9). We recommend this combination for the following reasons. First, each of the three substrates greatly influences the assessment of EDEMP fluxes via novel sugar labelling (Figs. 4, 8 and 9). Second, [1–^{13}C] glucose and [[13]C$_6$] glucose additionally provide resolution power to infer fluxes around the oxidative PP pathway, at the PYR node and around the TCA cycle via amino acid labelling (Wittmann and Heinzle, 2001b). Third, all substrates are commercially accessible at a reasonable price. However, the sensitivity observed in sugars is
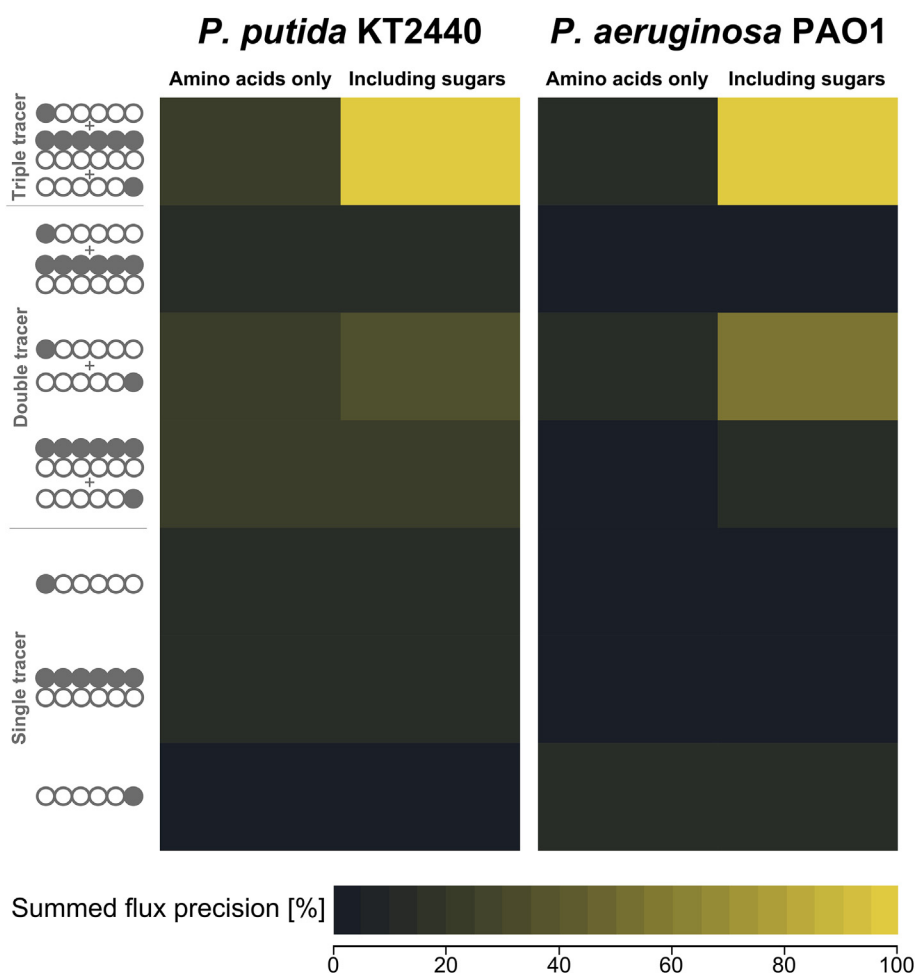
Fig. 9. Precision scores of different setups using GC-MS-based ^{13}C metabolic flux analysis of *Pseudomonas putida* KT2440 and *Pseudomonas aeruginosa* PAO1.

relatively independent from the chosen tracers (Figs. 4, S3, and S4), indicating that other combinations of tracers might also work.

P. aeruginosa PAO1 fluxes have not been previously analysed with such detail and accuracy, and they are discussed below in more detail. Regarding *P. putida* KT2440, the observed flux distribution exhibits high similarity to that of recent LC-MS-based flux studies (Nikel et al., 2015; Sasnow et al., 2016). This observation holds, e.g., for the strong preference of periplasmic oxidation over cytoplasmic phosphorylation at the entry of glucose into metabolism, the extremely low flux through the oxidative PP pathway, the high flux through the ED pathway, the active operation of the EDEMP cycle for triose recycling from G3P, the cyclic interconversion of carbon between C_3 units of the glycolysis and C_4 units of the TCA cycle, and the absence of the glyoxylate shunt (Fig. 6). Small differences in some of the fluxes can be attributed to differences in culture conditions and growth physiology. The overall high agreement together with the excellent goodness of fit (Fig. 5) can be taken as solid evidence that our developed strategy provides accurate flux values.

Approximately 200 species belong to the *Pseudomonas* genus. Among them are members of particular relevance and impact. For example, *P. putida* KT2440 and related strains are cell factories widely used for the production of various value-added products from renewables and even waste (Beckers et al., 2016; Belda et al., 2016; Borrero-de Acuña et al., 2017; Johnson et al., 2016; Kohlstedt et al., 2018; Kuepper et al., 2015; Martinez-Garcia et al., 2014; Nikel and de Lorenzo, 2013; Nikel and de Lorenzo, 2014; Poblete-Castro et al., 2013; Schmitz et al., 2015). *P. fluorescens* has found applications for bioconversions (Brunner et al., 2018) and as a plant-growth promoting bacterium (;Park et al., 2015; Prabhukarthikeyan et al., 2018). *Pseudomonas stutzeri* can be applied to degrade environmental pollutants (Saikia et al., 2005) and has recently received increasing interest for the production of membrane proteins (Sommer et al., 2017). Moreover, the genus comprises important human pathogens, such as *P. aeruginosa*, responsible for urinary-tract infections, cystic fibrosis, meningitis, and pneumonia (Gellatly and Hancock, 2013), and *Pseudomonas syringae*, a very important plant pathogen (Xin et al., 2018), both of which pose severe health threats to our society. Our novel approach renders all these interesting microbes more easily accessible on the flux level.

4.2. The novel approach overcomes the limitations of previous workflows for metabolic flux analysis of pseudomonads

Conventional flux analysis of pseudomonads uses GC-MS analysis of proteinogenic amino acids, as exemplified for *P. putida* (Blank et al., 2008; Ebert et al., 2011; Zobel et al., 2017), *Pseudomonas fluorescens* (Fuhrer et al., 2005), and *P. aeruginosa* (Berger et al., 2014; Lassek et al., 2016; Opperman and Shachar-Hill, 2016). While such studies provide a basic understanding of the investigated microbes, they fail to resolve a key part of metabolism, i.e., the EDEMP cycle, which merges activities belonging to the EMP pathway, the ED pathway, and the PP pathway into a complex architecture (Fig. 1). This failure is because the circular operation of these pathways does not cause sufficiently observable changes in the labelling pattern of the proteinogenic amino acids (Blank et al., 2008), as shown systematically in this work (Fig. 3). This inherent lack of sensitivity allows us to study glucose catabolism in pseudomonads via common workflows in only a simplified form: the different catabolic routes for glucose have to be lumped, and the total influx of the substrate is assigned to enter the G6P node (Berger et al., 2014; Ebert et al., 2011). This simplification, unfortunately, cannot address important questions about redox and energy metabolism (Blank et al., 2008; Ebert et al., 2011). The impact becomes obvious when the flux distributions around the glucose split in the resolved form and the unresolved form are compared (Fig. 10): both differ substantially. The simplified network provides a quite unrealistic picture regarding energy and redox: it overestimates ATP consumption and NADPH formation by a factor of two. In other cases, simplified approaches have even led to a

severe misinterpretation of data, an example being the wrongly determined high flux through the oxidative PP pathway in glucose-grown *P. aeruginosa* PAO1 (Opperman and Shachar-Hill, 2016), which, in fact, is practically absent (Fig. 7). Such limitations can be easily avoided and overcome using the described setup.

The approach presented in this study offers direct quantification of labelling patterns of the analytes of interest from complex biomass hydrolysates (Table 1 and Fig. 2). As shown, all labelling measurements can be performed on one single GC-MS instrument without any change in instrumental settings (e.g., injector, liner, GC separation column, and carrier gas) except for the temperature gradient, whose settings can be easily adapted (Table 1). Favourably, GC-MS instruments are robust, particularly easy to operate and maintain, and significantly less costly than other types of mass spectrometers or NMR instruments (Wittmann, 2007). Moreover, the amino acids and the sugars in the hydrolysates, as measured here, are very stable, indicating that the storage and shipping of samples would be straightforward. Due to these advantages, we conclude that our approach will stimulate and intensify future analysis of pseudomonad fluxes. In comparison, LC-MS-based flux studies based on intracellular metabolites are linked to a significant increase in experimental difficulty (Wiechert and Nöh, 2013). In particular, they require sophisticated cultivation protocols because even small changes in culture conditions, which are difficult to fully control in routine experiments, can immediately impact the labelling status of the intracellular pools and thus the outcome of such studies (Krömer et al., 2004; Nöh et al., 2007). Moreover, elaborate quenching and extraction protocols are needed to conserve the labelling patterns of the free metabolites in their *in vivo* state, which are rapidly changing, present at low concentrations, and partly unstable (Bolten et al., 2007; Long et al., 2016; Wittmann et al., 2005). We would, however, like to emphasize that we still regard the established LC-MS-based approaches as valuable and informative. As an example, they are superior in investigating flux dynamics (Wiechert and Nöh, 2013). Both types of studies will be useful in the future, and it will be up to the researcher to choose the most suitable method to address his or her specific question.

4.3. The glucosamine moiety of cellular carbohydrates refines flux resolution

Similar to our work, flux studies in other microbes have benefited from using labelling measurements in addition to common amino acid profiles. For example, the resolution of net and exchange fluxes in the oxidative PP pathway of *C. glutamicum* is improved by additional analysis of the G6P pool (Wittmann and Heinzle, 2001b), and this improved resolution was obtained in different flux studies of the microbe via GC-MS analysis of extracellular trehalose (Becker et al., 2007; Buschke et al., 2013; Wittmann and Heinzle, 2001a). In different sucrose-grown microbes, the G6P labelling is important for identifying and accurately observing fluxes due to the highly complex network reactions involved in sucrose catabolism and has been obtained from cellular glycogen (Lange et al., 2017) and secreted trehalose (Wittmann et al., 2004). Further refinement of PP pathway flux resolution in *E. coli* and in mammalian cells was achieved by combining information from the glucose moiety of glycogen and the ribose moiety of DNA (Long et al., 2016). Here, we propose the glucosamine moiety from peptidoglycan and lipopolysaccharides, representing F6P, as a novel fragment to be considered in flux analysis. Added together with the labelling of glucose to that of the amino acids, it enables high precision flux analysis of *P. putida* and *P. aeruginosa*. As shown, two clean glucose fragments (m/z 554 and m/z 319) and three clean glucosamine fragments (m/z 553, m/z 319, and m/z 159) contribute 81 mass isotopomer fractions to a total of 534 mass isotopomer fractions in a triple tracer set-up for flux estimation. The F6P pool is of specific importance in pseudomonads, where it is simultaneously supplied from three inflowing reactions, whose are catalyzed by phosphoglucoisomerase, fructose 1,6-bisphosphatase (triose recycling), and transaldolase (from
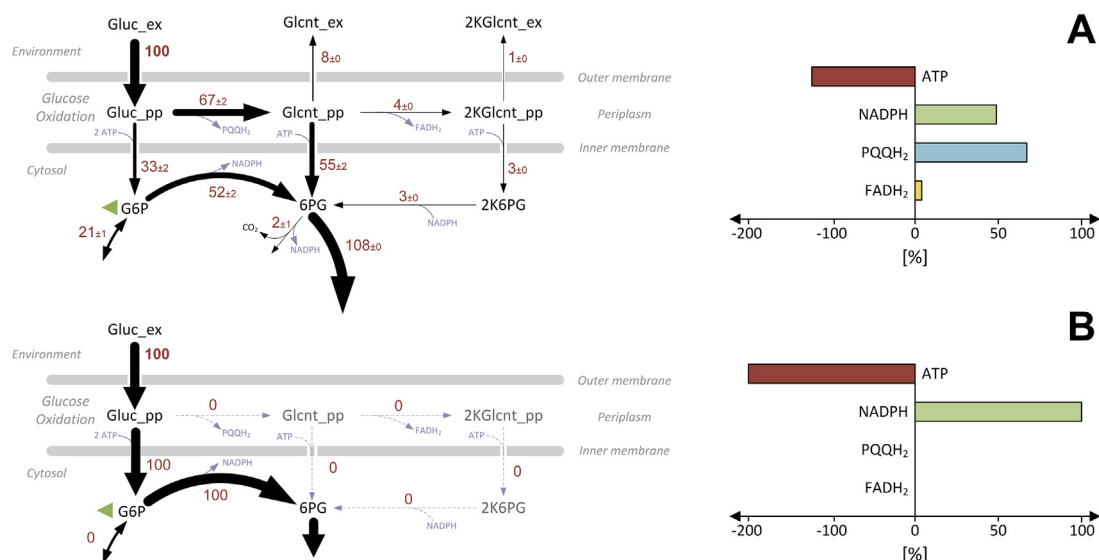
Fig. 10. Metabolic flux resolution of glucose catabolism in *Pseudomonas putida* KT2440 and its impact on physiological conclusions. Fluxes obtained from the high-resolution approach with consideration of amino acid and sugar labelling (A) and fluxes obtained from the low-resolution approach with consideration of amino acid and sugar labelling and lumped glucose catabolism (B).

the reversible non-oxidative PP pathway) (Fig. 1). As we show (Table S3), the F6P labelling differs significantly from that of G6P and (due to its prominent position in the network) responds differently in the sensitivity analysis (Fig. 4). Parameter estimations, which consider the F6P, G6P and amino acid labelling, result in significantly lower flux errors (Fig. S6), as compared to estimations without F6P. This observation underlines the importance of the newly introduced fragment to study microbes, which operate the EDEMP cycle.

It is difficult to predict the general impact of the glucosamine labelling on the outcome of flux analysis in other cells, which operate a functional EMP pathway. Eventually, the consideration of the G6P and the F6P labelling together could increase the accuracy to determine the reversibility of G6P isomerase, which interconverts these two metabolites at the entry into the EMP pathway. This in turn would help to even more precisely estimate the oxidative PP pathway flux, which depends on a solid estimate of the flux reversibility of G6P isomerase (Wittmann and Heinzle, 2001b). In this regard, it could be worth adding this labelling to recently developed workflows, although they offer a certain precision already (Long et al., 2016). Similarly, flux studies in sucrose-grown microbes, which form differently labelled units of F6P and G6P from the substrate, could likely benefit from additional glucosamine labelling analysis (Lange et al., 2017).

4.4. Glucose-grown P. putida generates a significant surplus of ATP

The obtained fluxes allow a closer inspection of the redox and energy metabolism of *P. putida* KT2440, providing a quantitative picture of NADPH as a central redox cofactor. When setting up a balance for NADPH, the supply results from the corresponding NADPH-dependent fluxes (Fig. 6), corrected for cofactor specificity under *in vivo* conditions (Nikel et al., 2015) (Fig. 11A). Anabolic NADPH consumption results from biomass-related demand (Nikel et al., 2015; van Duuren et al., 2013) and the measured specific growth rate (Table 1). In line with recent observations (Nikel et al., 2015), *P. putida* generates a slight catabolic excess of NADPH. The enzyme mainly supplying NADPH in this organism is isocitrate dehydrogenase, which is different from the situation in other microbes (Becker et al., 2011). The apparent surplus of NADPH is obviously converted into NADH via the activities of soluble (SthA) and membrane-bound, proton-translocating (PntAB) pyridine nucleotide transhydrogenases (Nikel et al., 2016).

Regarding energy metabolism, the ATP synthesized from NADH,

FADH$_2$ and PQQH$_2$ via oxidative phosphorylation in the respiratory chain is inferred from the formation of the reduced cofactors, considering the estimated fluxes (Fig. 6), cofactor specificity (Nikel et al., 2015) and the conversion of these three molecules into ATP assuming a P/O ratio of 1.875 for NADH and PQQH$_2$ (Hardy et al., 1993; Oberhardt et al., 2011) and 1.0 for FADH$_2$ (Yuan et al., 2017). In addition, ATP production results from substrate-level phosphorylation, i.e., ATP-producing and ATP-consuming fluxes (Fig. 6). On the other hand, the ATP demand is obtained by adding up the requirements for anabolism and non-growth-associated maintenance (NGAM) (Oberhardt et al., 2011; van Duuren et al., 2013; Yuan et al., 2017). *P. putida* supplies most ATP via oxidation of NADH (Fig. 11B). In addition, periplasmic metabolism contributes significantly to the organism's energy supply, whereas substrate-level phosphorylation is of minor relevance. Most energy is withdrawn for anabolism. In comparison, uptake of the substrate requires less energy, which is enabled by the fact that *P. putida* channels most glucose into metabolism through the periplasm, which costs only 1 ATP per glucose (Fig. 1). In this way the cell avoids the costly two-step route of glucose uptake into the cytoplasm via an ABC transporter and subsequent phosphorylation, which requires two molecules of ATP per molecule of glucose (Fig. 6). Taking these results together, *P. putida* KT2440 generates a large apparent surplus of ATP. This surplus is available to cover the ATP demand for growth-associated maintenance (GAM), which can vary substantially depending on growth conditions (Yuan et al., 2017). Moreover, it could be beneficial under stress and contribute to the excellent survival and robustness of the microbe (Belda et al., 2016; Kohlstedt et al., 2018; Nikel and de Lorenzo, 2014).

4.5. Glucose-grown P. aeruginosa PAO1 does not operate a functional oxidative pentose phosphate pathway in vivo

The central hub of glucose catabolism in *P. aeruginosa* PAO1 is 6PG (Fig. 7). The cells exclusively convert 6PG via the ED pathway. Strikingly, they do not use the alternative route via 6PG dehydrogenase and therefore obviously do not operate an active oxidative PP pathway under the conditions examined here. In contrast, a recent study inferred a strong flux through 6PG dehydrogenase and described the oxidative PP pathway as an important route of glucose catabolism in *P. aeruginosa* PAO1 (Opperman and Shachar-Hill, 2016). An inspection of the previous setup together with the simulation data of our work (Fig. 4) revealed that the measured amino acid labelling was likely not suitable in
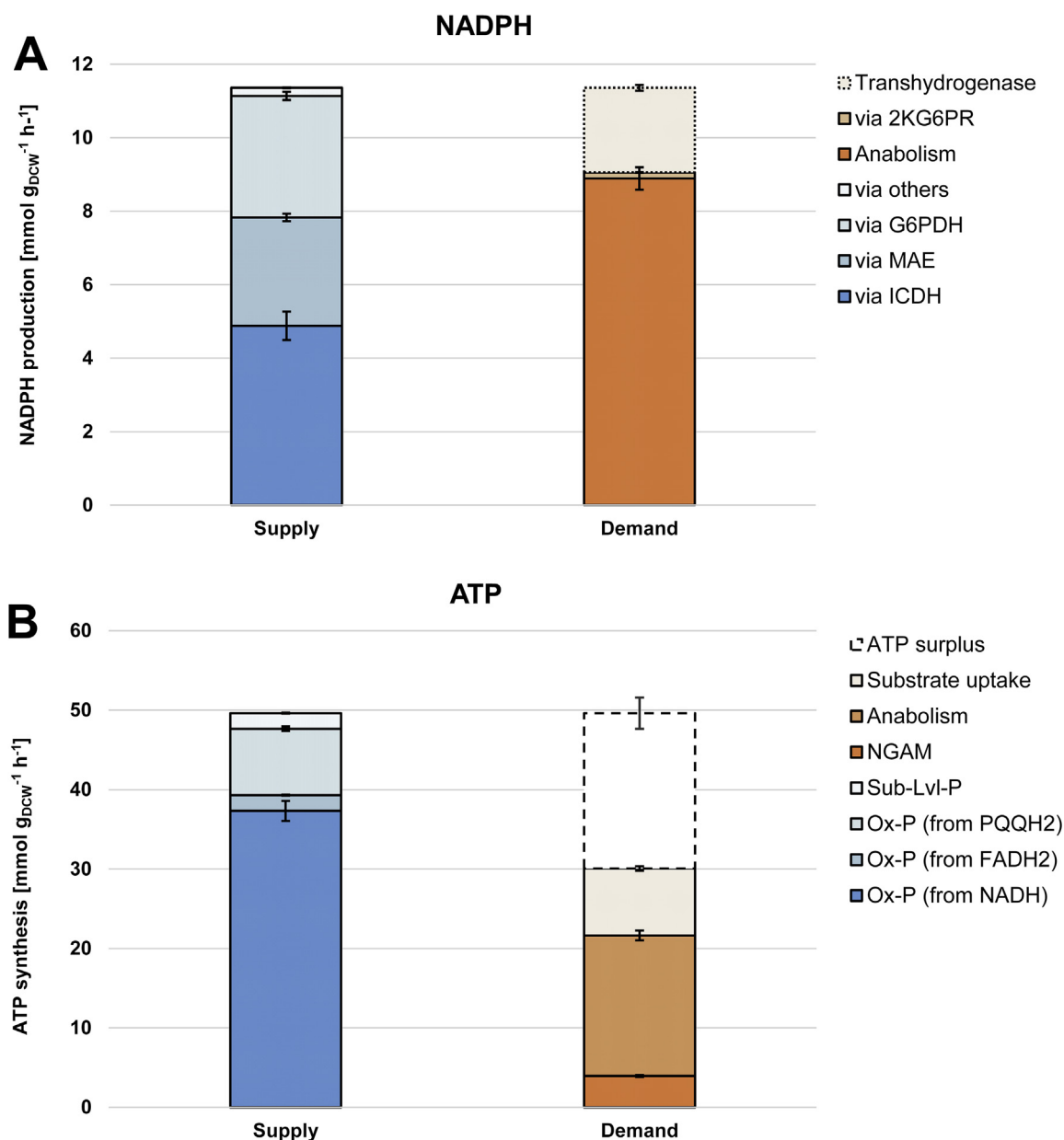
Fig. 11. Quantitative analysis of the redox and energy metabolism in glucose-grown *Pseudomonas putida* KT2440. Reactions linked to NADPH (A) and ATP (B) metabolism are calculated from the obtained fluxes (Fig. 6). They are given as absolute fluxes (mmol g_{DCW}^{-1} h^{-1}) and are related to the specific glucose uptake rate (Table 1).

resolving the fluxes. Moreover, the previous study obviously considered G6P and F6P as a single pool in the isotopomer network. On basis of our findings, this simplification was unfortunate. The two pools differ significantly in labelling (Table S3) and respond differently in the sensitivity simulations (Fig. 3), which results from their different positions within the network, and they should therefore be kept separate to avoid miscalculations.

Accordingly, the previous picture should be revised: the ED pathway is the major and perhaps even exclusive pathway for glucose breakdown in *P. aeruginosa* PAO1. Importantly, 6PG dehydrogenase activity has never been reported in fractionated extracts of *P. aeruginosa*, as would be expected were an authentic 6PG dehydrogenase present, suggesting the absence of this enzymatic activity; this absence is further supported by the data we present here (Lessie and Phibbs, 1984). In fact, a serine dehydrogenase that has no proven activity on 6PG was recently associated with this function (Bartell et al., 2017). Generally, the lack of a functional oxidative PP pathway, as shown here, would

have strong implications for our understanding of the cellular physiology of *P. aeruginosa* PAO1, particularly its fight against oxidative stress imposed by the infected host (Opperman and Shachar-Hill, 2016): other pathways would have to supply the antioxidant redox power (NADPH) in the absence of an active oxidative PP pathway. More work will be needed to completely address this question, particularly in clinical isolates that might differ in their genomic repertoire and exhibit a certain flexibility in pathway usage (Berger et al., 2014).

5. Conclusions

The approach presented here allows accurate, precise and convenient ^{13}C MFA of pseudomonads and related microbes possessing a parallel and convergent glucose intake and a cyclic organization of the hexose metabolism. The use of a single analytical platform (GC-MS) with only one chromatographic column and simple, robust protocols for sample preparation and processing opens the possibility to easily and

successfully conduct such studies in different laboratories. Flux analysis of *Pseudomonas*, as well as a surprisingly large number of microbes that likely utilize the EDEMP cycle during hexose metabolism (Flamholz et al., 2013; Fürch et al., 2009; Klingner et al., 2015), becomes more accessible using the presented approach, representing a valuable extension of the available set of flux methods for these types of bacteria.

Acknowledgements

Appendix A. Supplementary data

Supplementary data to this article can be found online at https://doi.org/10.1016/j.ymben.2019.01.008.

References

Adler, P., Bolten, C.J., Dohnt, K., Hansen, C.E., Wittmann, C., 2013. Core fluxome and metafluxome of lactic acid bacteria under simulated cocoa pulp fermentation conditions. Appl. Environ. Microbiol. 79, 5670–5681.

Barbier, T., Collard, F., Zuniga-Ripa, A., Moriyon, I., Godard, T., Becker, J., Wittmann, C., Van Schaftingen, E., Letesson, J.J., 2014. Erythritol feeds the pentose phosphate pathway via three new isomerases leading to D-erythrose-4-phosphate in *Brucella*. Proc. Natl. Acad. Sci. Unit. States Am. 111, 17815–17820.

Bartek, T., Blombach, B., Lang, S., Eikmanns, B.J., Wiechert, W., Oldiges, M., Nöh, K., Noack, S., 2011. Comparative ^{13}C metabolic flux analysis of pyruvate dehydrogenase complex-deficient, L-valine-producing *Corynebacterium glutamicum*. Appl. Environ. Microbiol. 77, 6644–6652.

Bartell, J.A., Blazier, A.S., Yen, P., Thogersen, J.C., Jelsbak, L., Goldberg, J.B., Papin, J.A., 2017. Reconstruction of the metabolic network of *Pseudomonas aeruginosa* to interrogate virulence factor synthesis. Nat. Commun. 8, 14631.

Becker, J., Klopprogge, C., Herold, A., Zelder, O., Bolten, C.J., Wittmann, C., 2007. Metabolic flux engineering of L-lysine production in *Corynebacterium glutamicum* – overexpression and modification of G6P dehydrogenase. J. Biotechnol. 132, 99–109.

Becker, J., Klopprogge, C., Wittmann, C., 2008. Metabolic responses to pyruvate kinase deletion in lysine producing *Corynebacterium glutamicum*. Microb. Cell Factories 7, 8.

Becker, J., Klopprogge, C., Zelder, O., Heinzle, E., Wittmann, C., 2005. Amplified expression of fructose 1,6-bisphosphatase in *Corynebacterium glutamicum* increases *in vivo* flux through the pentose phosphate pathway and lysine production on different carbon sources. Appl. Environ. Microbiol. 71, 8587–8596.

Becker, J., Reinefeld, J., Stellmacher, R., Schäfer, R., Lange, A., Meyer, H., Lalk, M., Zelder, O., von Abendroth, G., Schröder, H., Haefner, S., Wittmann, C., 2013. Systems-wide analysis and engineering of metabolic pathway fluxes in bio-succinate producing *Basfia succiniciproducens*. Biotechnol. Bioeng. 110, 3013–3023.

Becker, J., Zelder, O., Haefner, S., Schröder, H., Wittmann, C., 2011. From zero to hero – design-based systems metabolic engineering of *Corynebacterium glutamicum* for L-lysine production. Metab. Eng. 13, 159–168.

Beckers, V., Poblete-Castro, I., Tomasch, J., Wittmann, C., 2016. Integrated analysis of gene expression and metabolic fluxes in PHA-producing *Pseudomonas putida* grown on glycerol. Microb. Cell Factories 15, 73.

Belda, E., van Heck, R.G., Jose Lopez-Sanchez, M., Cruveiller, S., Barbe, V., Fraser, C., Klenk, H.P., Petersen, J., Morgat, A., Nikel, P.I., Vallenet, D., Rouy, Z., Sekowska, A., Martins Dos Santos, V.A., de Lorenzo, V., Danchin, A., Medigue, C., 2016. The revisited genome of *Pseudomonas putida* KT2440 enlightens its value as a robust metabolic chassis. Environ. Microbiol. 18, 3403–3424.

Berger, A., Dohnt, K., Tielen, P., Jahn, D., Becker, J., Wittmann, C., 2014. Robustness and plasticity of metabolic pathway flux among uropathogenic isolates of *Pseudomonas aeruginosa*. PLoS One 9, e88368.

Beste, D.J.V., Bonde, B., Hawkins, N., Ward, J.L., Beale, M.H., Noack, S., Nöh, K., Kruger, N.J., Ratcliffe, R.G., McFadden, J., 2011. [13]C metabolic flux analysis identifies an unusual route for pyruvate dissimilation in mycobacteria which requires isocitrate lyase and carbon dioxide fixation. PLoS Pathog. 7.

Blank, L.M., Ionidis, G., Ebert, B.E., Buhler, B., Schmid, A., 2008. Metabolic response of *Pseudomonas putida* during redox biocatalysis in the presence of a second octanol phase. FEBS J. 275, 5173–5190.

Boisseau, R., Charrier, B., Massou, S., Portais, J.C., Akoka, S., Giraudeau, P., 2013. Fast spatially encoded 3D NMR strategies for ^{13}C-based metabolic flux analysis. Anal. Chem. 85, 9751–9757.

Bolten, C.J., Kiefer, P., Letisse, F., Portais, J.C., Wittmann, C., 2007. Sampling for metabolome analysis of microorganisms. Anal. Chem. 79, 3843–3849.

Borrero-de Acuña, J.M., Hidalgo-Dumont, C., Pacheco, N., Cabrera, A., Poblete-Castro, I.,

2017. A novel programmable lysozyme-based lysis system in *Pseudomonas putida* for biopolymer production. Sci. Rep. 7, 4373.

Brunner, S., Eppinger, E., Fischer, S., Groning, J., Stolz, A., 2018. Conversion of aliphatic nitriles by the arylacetonitrilase from *Pseudomonas fluorescens* EBC191. World J. Microbiol. Biotechnol. 34, 91.

Bücker, R., Heroven, A.K., Becker, J., Dersch, P., Wittmann, C., 2014. The pyruvate-tricarboxylic acid cycle node: a focal point of virulence control in the enteric pathogen *Yersinia pseudotuberculosis*. J. Biol. Chem. 289, 30114–30132.

Buescher, J.M., Antoniewicz, M.R., Boros, L.G., Burgess, S.C., Brunengraber, H., Clish, C.B., DeBerardinis, R.J., Feron, O., Frezza, C., Ghesquiere, B., Gottlieb, E., Hiller, K., Jones, R.G., Kamphorst, J.J., Kibbey, R.G., Kimmelman, A.C., Locasale, J.W., Lunt, S.Y., Maddocks, O.D., Malloy, C., Metallo, C.M., Meuillet, E.J., Munger, J., Nöh, K., Rabinowitz, J.D., Ralser, M., Sauer, U., Stephanopoulos, G., St-Pierre, J., Tennant, D.A., Wittmann, C., Vander Heiden, M.G., Vazquez, A., Vousden, K., Young, J.D., Zamboni, N., Fendt, S.M., 2015. A roadmap for interpreting ^{13}C metabolite labeling patterns from cells. Curr. Opin. Biotechnol. 34C, 189–201.

Buschke, N., Becker, J., Schäfer, R., Kiefer, P., Biedendieck, R., Wittmann, C., 2013. Systems metabolic engineering of xylose-utilizing *Corynebacterium glutamicum* for production of 1,5-diaminopentane. Biotechnol. J. 8, 557–570.

Chavarría, M., Kleijn, R.J., Sauer, U., Pflüger-Grau, K., de Lorenzo, V., 2012. Regulatory tasks of the phosphoenolpyruvate-phosphotransferase system of Pseudomonas putida in central carbon metabolism. mBio 3 e00028–12.

Choudhary, M.K., Yoon, J.M., Gonzalez, R., Shanks, J.V., 2011. Re-examination of metabolic fluxes in *Escherichia coli* during anaerobic fermentation of glucose using ^{13}C labeling experiments and 2-dimensional nuclear magnetic resonance (NMR) spectroscopy. Biotechnol. Bioproc. Eng. 16, 419–437.

Christensen, B., Thykaer, J., Nielsen, J., 2000. Metabolic characterization of high- and low-yielding strains of *Penicillium chrysogenum*. Appl. Microbiol. Biotechnol. 54, 212–217.

Crown, S.B., Antoniewicz, M.R., 2013. Parallel labeling experiments and metabolic flux analysis: past, present and future methodologies. Metab. Eng. 16, 21–32.

Dauner, M., Sauer, U., 2000. GC-MS analysis of amino acids rapidly provides rich information for isotopomer balancing. Biotechnol. Prog. 16, 642–649.

del Castillo, T., Ramos, J.L., Rodriguez-Herva, J.J., Fuhrer, T., Sauer, U., Duque, E., 2007. Convergent peripheral pathways catalyze initial glucose catabolism in *Pseudomonas putida*: genomic and flux analysis. J. Bacteriol. 189, 5142–5152.

Ebert, B.E., Kurth, F., Grund, M., Blank, L.M., Schmid, A., 2011. Response of *Pseudomonas putida* KT2440 to increased NADH and ATP demand. Appl. Environ. Microbiol. 77, 6597–6605.

Entner, N., Doudoroff, M., 1952. Glucose and gluconic acid oxidation of *Pseudomonas saccharophila*. J. Biol. Chem. 196, 853–862.

Fischer, E., Sauer, U., 2003. Metabolic flux profiling of *Escherichia coli* mutants in central carbon metabolism using GC-MS. Eur. J. Biochem. 270, 880–891.

Flamholz, A., Noor, E., Bar-Even, A., Liebermeister, W., Milo, R., 2013. Glycolytic strategy as a tradeoff between energy yield and protein cost. Proc. Natl. Acad. Sci. U. S. A 110, 10039–10044.

Fuhrer, T., Fischer, E., Sauer, U., 2005. Experimental identification and quantification of glucose metabolism in seven bacterial species. J. Bacteriol. 187, 1581–1590.

Fürch, T., Preusse, M., Tomasch, J., Zech, H., Wagner-Döbler, I., Rabus, R., Wittmann, C., 2009. Metabolic fluxes in the central carbon metabolism of *Dinoroseobacter shibae* and *Phaeobacter gallaeciensis*, two members of the marine Roseobacter clade. BMC Microbiol. 9, 209.

Gellatly, S.L., Hancock, R.E.W., 2013. *Pseudomonas aeruginosa*: new insights into pathogenesis and host defenses. Pathog. Dis. 67, 159–173.

Gosselin, I., Wattraint, O., Riboul, D., Barbotin, J.N., Portais, J.C., 2001. A deeper investigation on carbohydrate cycling in *Sinorhizobium meliloti*. FEBS Lett. 499, 45–49.

Hardy, G.P.M.A., Demattos, M.J.T., Neijssel, O.M., 1993. Energy conservation by pyrroloquinoline quinol-linked xylose oxidation in *Pseudomonas putida* NCTC 10936 during carbon-limited growth in chemostat culture. FEMS Microbiol. Lett. 107, 107–110.

Hayakawa, K., Matsuda, F., Shimizu, H., 2018. ^{13}C-metabolic flux analysis of ethanol-assimilating *Saccharomyces cerevisiae* for *S*-adenosyl-L-methionine production. Microb. Cell Factories 17.

He, L., Xiu, Y., Jones, J.A., Baidoo, E.E.K., Keasling, J.D., Tang, Y.J., Koffas, M.A.G., 2017. Deciphering flux adjustments of engineered *E. coli* cells during fermentation with changing growth conditions. Metab. Eng. 39, 247–256.

Heinzle, E., Yuan, Y., Kumar, S., Wittmann, C., Gehre, M., Richnow, H.H., Wehrung, P., Adam, P., Albrecht, P., 2008. Analysis of ^{13}C labeling enrichment in microbial culture applying metabolic tracer experiments using gas chromatography-combustion-isotope ratio mass spectrometry. Anal. Biochem. 380, 202–210.

Hoffmann, S.L., Jungmann, L., Schiefelbein, S., Peyriga, L., Cahoreau, E., Portais, J.C., Becker, J., Wittmann, C., 2018. Lysine production from the sugar alcohol mannitol: design of the cell factory *Corynebacterium glutamicum* SEA-3 through integrated analysis and engineering of metabolic pathway fluxes. Metab. Eng. 47, 475–487.

Johnson, C.W., Salvachua, D., Khanna, P., Smith, H., Peterson, D.J., Beckham, G.T., 2016. Enhancing muconic acid production from glucose and lignin-derived aromatic compounds via increased protocatechuate decarboxylase activity. Metab. Eng. Commun. 3, 111–119.

Kiefer, P., Heinzle, E., Zelder, O., Wittmann, C., 2004. Comparative metabolic flux analysis of lysine-producing *Corynebacterium glutamicum* cultured on glucose or fructose. Appl. Environ. Microbiol. 70, 229–239.

Kind, S., Becker, J., Wittmann, C., 2013. Increased lysine production by flux coupling of the tricarboxylic acid cycle and the lysine biosynthetic pathway–metabolic engineering of the availability of succinyl-CoA in *Corynebacterium glutamicum*. Metab. Eng. 15, 184–195.

Klingner, A., Bartsch, A., Dogs, M., Wagner-Döbler, I., Jahn, D., Simon, M., Brinkhoff, T., Becker, J., Wittmann, C., 2015. Large-scale ^{13}C flux profiling reveals conservation of

the Entner-Doudoroff pathway as a glycolytic strategy among marine bacteria that use glucose. Appl. Environ. Microbiol. 81, 2408–2422.

Kohlstedt, M., Sappa, P.K., Meyer, H., Maaß, S., Zaprasis, A., Hoffmann, T., Becker, J., Steil, L., Hecker, M., van Dijl, J.M., Lalk, M., Mäder, U., Stülke, J., Bremer, E., Völker, U., Wittmann, C., 2014. Adaptation of *Bacillus subtilis* carbon core metabolism to simultaneous nutrient limitation and osmotic challenge: a multi-omics perspective. Environ. Microbiol. 16, 1898–1917.

Kohlstedt, M., Starck, S., Barton, N., Stolzenberger, J., Selzer, M., Mehlmann, K., Schneider, R., Pleissner, D., Rinkel, J., Dickschat, J.S., Venus, J., van Duuren, J.B.J.H., Wittmann, C., 2018. From lignin to nylon: cascaded chemical and bio-chemical conversion using metabolically engineered *Pseudomonas putida*. Metab. Eng. 47, 279–293.

Krömer, J.O., Sorgenfrei, O., Klopprogge, K., Heinzle, E., Wittmann, C., 2004. In-depth profiling of lysine-producing *Corynebacterium glutamicum* by combined analysis of the transcriptome, metabolome, and fluxome. J. Bacteriol. 186, 1769–1784.

Kuepper, J., Dickler, J., Biggel, M., Behnken, S., Jäger, G., Wierckx, N., Blank, L.M., 2015. Metabolic engineering of *Pseudomonas putida* KT2440 to produce anthranilate from glucose. Front. Microbiol. 6, 1310.

LaBauve, A.E., Wargo, M.J., 2012. Growth and laboratory maintenance of *Pseudomonas aeruginosa*. In: Current Protocols in Microbiology, (Chapter 6), Unit 6E 1.

Lange, A., Becker, J., Schulze, D., Cahoreau, E., Portais, J.C., Haefner, S., Schröder, H., Krawczyk, J., Zelder, O., Wittmann, C., 2017. Bio-based succinate from sucrose: high-resolution ^{13}C metabolic flux analysis and metabolic engineering of the rumen bac-terium *Basfia succiniciproducens*. Metab. Eng. 44, 198–212.

Lassek, C., Berger, A., Zühlke, D., Wittmann, C., Riedel, K., 2016. Proteome and carbon flux analysis of *Pseudomonas aeruginosa* clinical isolates from different infection sites. Proteomics 16, 1381–1385.

Lee, S.Y., Kim, T.Y., 2005. Improving metabolic flux analysis by reconciliation of GC/MS based flux distribution data. Abstr. Pap. Am. Chem. Soc. 229 U224-U224.

Lehnen, M., Ebert, B.E., Blank, L.M., 2017. A comprehensive evaluation of constraining amino acid biosynthesis in compartmented models for metabolic flux analysis. Metab. Eng. Commun. 5, 34–44.

Lessie, T.G., Phibbs, P.V., 1984. Alternative pathways of carbohydrate utilization in pseudomonads. Annu. Rev. Microbiol. 38, 359–387.

Long, C.P., Au, J., Gonzalez, J.E., Antoniewicz, M.R., 2016. ^{13}C metabolic flux analysis of microbial and mammalian systems is enhanced with GC-MS measurements of gly-cogen and RNA labeling. Metab. Eng. 38, 65–72.

Long, C.P., Gonzalez, J.E., Cipolla, R.M., Antoniewicz, M.R., 2017. Metabolism of the fast-growing bacterium *Vibrio natriegens* elucidated by ^{13}C metabolic flux analysis. Metab. Eng. 44, 191–197.

Martínez-García, E., Nikel, P.I., Aparicio, T., de Lorenzo, V., 2014. *Pseudomonas* 2.0: genetic upgrading of *P. putida* KT2440 as an enhanced host for heterologous gene expression. Microb. Cell Factories 13, 159.

Michal, G., 1999. Biochemical Pathways. John Wiley & Sons Inc.

Millard, P., Cahoreau, E., Heuillet, M., Portais, J.C., Lippens, G., 2017. ^{15}N-NMR-based approach for amino acids-based ^{13}C-metabolic flux analysis of metabolism. Anal. Chem. 89, 2101–2106.

Nelson, K.E., Weinel, C., Paulsen, I.T., Dodson, R.J., Hilbert, H., Martins dos Santos, V.A., Fouts, D.E., Gill, S.R., Pop, M., Holmes, M., Brinkac, L., Beanan, M., DeBoy, R.T., Daugherty, S., Kolonay, J., Madupu, R., Nelson, W., White, O., Peterson, J., Khouri, H., Hance, I., Chris Lee, P., Holtzapple, E., Scanlan, D., Tran, K., Moazzez, A., Utterback, T., Rizzo, M., Lee, K., Kosack, D., Moestl, D., Wedler, H., Lauber, J., Stjepandic, D., Hoheisel, J., Straetz, M., Heim, S., Kiewitz, C., Eisen, J.A., Timmis, K.N., Düsterhöft, A., Tümmler, B., Fraser, C.M., 2002. Complete genome sequence and comparative analysis of the metabolically versatile *Pseudomonas putida* KT2440. Environ. Microbiol. 4, 799–808.

Nikel, P.I., 2016. Systems and synthetic biology approaches for metabolic engineering of *Pseudomonas putida*. Microbial. Model. Environ. Ind. Sustain. 1, 3–22.

Nikel, P.I., Chavarría, M., Fuhrer, T., Sauer, U., de Lorenzo, V., 2015. *Pseudomonas putida* KT2440 strain metabolizes glucose through a cycle formed by enzymes of the Entner-Doudoroff, Embden-Meyerhof-Parnas, and pentose phosphate pathways. J. Biol. Chem. 290, 25920–25932.

Nikel, P.I., de Lorenzo, V., 2013. Engineering an anaerobic metabolic regime in *Pseudomonas putida* KT2440 for the anoxic biodegradation of 1,3-dichloroprop-1-ene. Metab. Eng. 15, 98–112.

Nikel, P.I., de Lorenzo, V., 2014. Robustness of *Pseudomonas putida* KT2440 as a host for ethanol biosynthesis. N. Biotech. 31, 562–571.

Nikel, P.I., Pérez-Pantoja, D., de Lorenzo, V., 2016. Pyridine nucleotide transhy-drogenases enable redox balance of *Pseudomonas putida* during biodegradation of aromatic compounds. Environ. Microbiol. 18, 3565–3582.

Nöh, K., Grönke, K., Luo, B., Takors, R., Oldiges, M., Wiechert, W., 2007. Metabolic flux analysis at ultra short time scale: isotopically non-stationary ^{13}C labeling experi-ments. J. Biotechnol. 129, 249–267.

Oberhardt, M.A., Puchałka, J., Martins dos Santos, V.A., Papin, J.A., 2011. Reconciliation of genome-scale metabolic reconstructions for comparative systems analysis. PLoS Comput. Biol. 7.

Opperman, M.J., Shachar-Hill, Y., 2016. Metabolic flux analyses of *Pseudomonas aerugi-nosa* cystic fibrosis isolates. Metab. Eng. 38, 251–263.

Ornston, M.K., Ornston, L.N., 1969. Two forms of D-glycerate kinase in *Escherichia coli*. J. Bacteriol. 97, 1227–1233.

Park, Y.S., Dutta, S., Ann, M., Raaijmakers, J.M., Park, K., 2015. Promotion of plant growth by Pseudomonas fluorescens strain SS101 via novel volatile organic com-pounds. Biochem. Bioph. Res. Commun. 461, 361–365.

Phibbs, P.V., Feary, T.W., Blevins, W.T., 1974. Pyruvate carboxylase deficiency in pleiotropic carbohydrate-negative mutant strains of *Pseudomonas aeruginosa*. J. Bacteriol. 118, 999–1009.

Poblete-Castro, I., Becker, J., Dohnt, K., Martins dos Santos, V.A., Wittmann, C., 2012. Industrial biotechnology of *Pseudomonas putida* and related species. Appl. Microbiol. Biotechnol. 93, 2279–2290.

Poblete-Castro, I., Binger, D., Rodrigues, A., Becker, J., Martins Dos Santos, V.A., Wittmann, C., 2013. In-silico-driven metabolic engineering of *Pseudomonas putida* for enhanced production of poly-hydroxyalkanoates. Metab. Eng. 15, 113–123.

Portais, J.C., Tavernier, P., Gosselin, I., Barbotin, J.N., 1999. Cyclic organization of the carbohydrate metabolism in *Sinorhizobium meliloti*. Eur. J. Biochem. 265, 473–480.

Prabhukarthikeyan, S.R., Keerthana, U., Raguchander, T., 2018. Antibiotic-producing *Pseudomonas fluorescens* mediates rhizome rot disease resistance and promotes plant growth in turmeric plants. Microbiol. Res. 210, 65–73.

Price, N.P., Whitehead, T.R., Cote, G.L., 2006. Gas chromatography-mass spectrometry (GC-MS) techniques for metabolic flux analysis of the *Bifido* shunt pathway. Biocatal. Biotransform. 24, 95–98.

Quek, L.E., Nielsen, L.K., 2014. Steady-State ^{13}C fluxomics using OpenFLUX. Methods Mol. Biol. 1191, 209–224.

Quek, L.E., Wittmann, C., Nielsen, L.K., Krömer, J.O., 2009. OpenFLUX: efficient mod-elling software for ^{13}C-based metabolic flux analysis. Microb. Cell Factories 8, 25.

Reardon, P.N., Isern, N.G., 2017. Fast multidimensional NMR for ^{13}C metabolic flux analysis. Emagres 6, 419–426.

Romano, A.H., Conway, T., 1996. Evolution of carbohydrate metabolic pathways. Res. Microbiol. 147, 448–455.

Saikia, N., Das, S.K., Patel, B.K.C., Niwas, R., Singh, A., Gopal, M., 2005. Biodegradation of beta-cyfluthrin by *Pseudomonas stutzeri* strain S1. Biodegradation 16, 581–589.

Sasnow, S.S., Wei, H., Aristilde, L., 2016. Bypasses in intracellular glucose metabolism in iron-limited *Pseudomonas putida*. MicrobiologyOpen 5, 3–20.

Schilling, O., Frick, O., Herzberg, C., Ehrenreich, A., Heinzle, E., Wittmann, C., Stülke, J., 2007. Transcriptional and metabolic responses of *Bacillus subtilis* to the availability of organic acids: transcription regulation is important but not sufficient to account for metabolic adaptation. Appl. Environ. Microbiol. 73, 499–507.

Schmitz, S., Nies, S., Wierckx, N., Blank, L.M., Rosenbaum, M.A., 2015. Engineering mediator-based electroactivity in the obligate aerobic bacterium *Pseudomonas putida* KT2440. Front. Microbiol. 6, 284.

Schwechheimer, S.K., Becker, J., Wittmann, C., 2018. Towards better understanding of industrial cell factories: novel approaches for ^{13}C metabolic flux analysis in complex nutrient environments. Curr. Opin. Biotechnol. 54, 128–137.

Shirai, T., Nakato, A., Izutani, N., Nagahisa, K., Shioya, S., Kimura, E., Kawarabayashi, Y., Yamagishi, A., Gojobori, T., Shimizu, H., 2005. Comparative study of flux redis-tribution of metabolic pathway in glutamate production by two coryneform bacteria. Metab. Eng. 7, 59–69.

Sommer, M., Xie, H., Michel, H., 2017. *Pseudomonas stutzeri* as an alternative host for membrane proteins. Microb. Cell Factories 16, 157.

Sudarsan, S., Dethlefsen, S., Blank, L.M., Siemann-Herzberg, M., Schmid, A., 2014. The functional structure of central carbon metabolism in *Pseudomonas putida* KT2440. Appl. Environ. Microbiol. 80, 5292–5303.

Tang, Y.J., Martin, H.G., Deutschbauer, A., Feng, X.Y., Huang, R., Llora, X., Arkin, A., Keasling, J.D., 2009. Invariability of central metabolic flux distribution in *Shewanella oneidensis* MR-1 under environmental or genetic perturbations. Biotechnol. Prog. 25, 1254–1259.

Tang, Y.J.J., Chakraborty, R., Martin, H.G., Chu, J., Hazen, T.C., Keasling, J.D., 2007. Flux analysis of central metabolic pathways in *Geobacter metallireducens* during re-duction of soluble Fe(III)-nitrilotriacetic acid. Appl. Environ. Microbiol. 73, 3859–3864.

Tlemçani, L.L., Corroler, D., Barillier, D., Mosrati, R., 2008. Physiological states and en-ergetic adaptation during growth of *Pseudomonas putida* mt-2 on glucose. Arch. Microbiol. 190, 141–150.

van Duuren, J.B.J.H., Puchałka, J., Mars, A.E., Bücker, R., Eggink, G., Wittmann, C., Martins dos Santos, V.A., 2013. Reconciling *in vivo* and *in silico* key biological para-meters of *Pseudomonas putida* KT2440 during growth on glucose under carbon-limited condition. BMC Biotechnol. 13, 93.

van Winden, W.A., Wittmann, C., Heinzle, E., Heijnen, J.J., 2002. Correcting mass iso-topomer distributions for naturally occurring isotopes. Biotechnol. Bioeng. 80, 477–479.

Vicente, M., Canovas, J.L., 1973. Glucolysis in *Pseudomonas putida*: physiological role of alternative routes from the analysis of defective mutants. J. Bacteriol. 116, 908–914.

Wada, K., Toya, Y., Banno, S., Yoshikawa, K., Matsuda, F., Shimizu, H., 2017. ^{13}C-me-tabolic flux analysis for mevalonate-producing strain of *Escherichia coli*. J. Biosci. Bioeng. 123, 177–182.

Wiechert, W., Nöh, K., 2013. Isotopically non-stationary metabolic flux analysis: complex yet highly informative. Curr. Opin. Biotechnol. 24, 979–986.

Wierckx, N., Ruijssenaars, H.J., de Winde, J.H., Schmid, A., Blank, L.M., 2009. Metabolic flux analysis of a phenol producing mutant of *Pseudomonas putida* S12: verification and complementation of hypotheses derived from transcriptomics. J. Biotechnol. 143, 124–129.

Wittmann, C., 2007. Fluxome analysis using GC-MS. Microb. Cell Factories 6, 6.

Wittmann, C., Hans, M., Heinzle, E., 2002. *In vivo* analysis of intracellular amino acid labelings by GC/MS. Anal. Biochem. 307, 379–382.

Wittmann, C., Hans, M., van Winden, W.A., Ras, C., Heijnen, J.J., 2005. Dynamics of intracellular metabolites of glycolysis and TCA cycle during cell-cycle-related oscil-lation in *Saccharomyces cerevisiae*. Biotechnol. Bioeng. 89, 839–847.

Wittmann, C., Heinzle, E., 2001a. Application of MALDI-TOF MS to lysine-producing *Corynebacterium glutamicum*: a novel approach for metabolic flux analysis. Eur. J. Biochem. FEBS 268, 2441–2455.

Wittmann, C., Heinzle, E., 2001b. Modeling and experimental design for metabolic flux analysis of lysine-producing corynebacteria by mass spectrometry. Metab. Eng. 3, 173–191.

Wittmann, C., Heinzle, E., 2002. Genealogy profiling through strain improvement by using metabolic network analysis: metabolic flux genealogy of several generations of lysine-producing corynebacteria. Appl. Environ. Microbiol. 68, 5843–5859.

Wittmann, C., Weber, J., Betiku, E., Krömer, J., Bohm, D., Rinas, U., 2007. Response of fluxome and metabolome to temperature-induced recombinant protein synthesis in *Escherichia coli*. J. Biotechnol. 132, 375–384.

Wittmann, C., Kiefer, P., Zelder, O., 2004. Metabolic fluxes in Corynebacterium glutamicum during lysine production with sucrose as carbon source. Appl. Environ. Microbiol. 70, 7277–7287.

Xin, X.F., Kvitko, B., He, S.Y., 2018. *Pseudomonas syringae*: what it takes to be a pathogen. Nat. Rev. Microbiol. 16, 316–328.

Yang, T.H., Wittmann, C., Heinzle, E., 2006. Respirometric ^{13}C flux analysis Part II: in vivo flux estimation of lysine-producing *Corynebacterium glutamicum*. Metab. Eng. 8, 432–446.

Yuan, Q.Q., Huang, T., Li, P.S., Hao, T., Li, F.R., Ma, H.W., Wang, Z.W., Zhao, X.M., Chen, T., Goryanin, I., 2017. Pathway consensus approach to metabolic network re-construction for *Pseudomonas putida* KT2440 by systematic comparison of published models. PLoS One 12.

Zamboni, N., Fendt, S.M., Rühl, M., Sauer, U., 2009. ^{13}C-based metabolic flux analysis. Nat. Protoc. 4, 878–892.

Zobel, S., Kuepper, J., Ebert, B., Wierckx, N., Blank, L.M., 2017. Metabolic response of *Pseudomonas putida* to increased NADH regeneration rates. Eng. Life Sci. 17, 47–57.